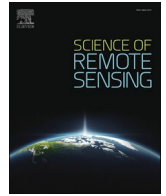


Contents lists available at [ScienceDirect](https://www.sciencedirect.com)

Science of Remote Sensing

journal homepage: www.sciencedirect.com/journal/science-of-remote-sensing

Comprehensive comparison of airborne and spaceborne SAR and LiDAR estimates of forest structure in the tallest mangrove forest on earth

Atticus E.L. Stovall^{a,b,*}, Temilola Fatoyinbo^a, Nathan M. Thomas^c, John Armston^b, Médard Obiang Ebanega^d, Marc Simard^e, Carl Trettin^f, Robert Vancelas Obiang Zogo^d, Igor Akendengue Aken^d, Michael Debina^e, Alphna Mekui Me Kemoe^d, Emmanuel Ondo Assoumou^d, Jun Su Kim^g, David Lagomasino^h, Seung-Kuk Leeⁱ, Jean Calvin Ndong Obame^g, Geldin Derrick Voubou^g, Chamberlain Zame Essono^g

^a NASA Goddard Space Flight Center, Greenbelt, MD, USA

^b Department of Geographical Sciences, University of Maryland, MD, USA

^c Earth System Science Interdisciplinary Science Center, University of Maryland, MD, USA

^d Omar Bongo University, Libreville, Gabon

^e Jet Propulsion Laboratory, California Institute of Technology, CA, USA

^f USDA Forest Service Southern Research Station, USA

^g German Aerospace Center (DLR), Microwaves and Radar Institute, 82234, Weßling, Germany

^h Department of Coastal Studies, East Carolina University, Wanchese, NC, USA

ⁱ Department of Earth and Environmental Sciences, Pukyong National University, Busan, South Korea

ARTICLE INFO

Keywords:

AfriSAR
Carbon
ALOS
SRTM
TanDEM-X
ICESat-2
GEDI
LVIS
F-SAR
UAVSAR
GEOCARBON
IPCC

ABSTRACT

A recent suite of new global-scale satellite sensors and regional-scale airborne campaigns are providing a wealth of remote sensing data capable of dramatically advancing our current understanding of the spatial distribution of forest structure and carbon stocks. However, a baseline for forest stature and biomass estimates has yet to be established for the wide array of available remote sensing products. At present, it remains unclear how the estimates from these sensors compare to one another in terrestrial forests, with a clear dearth of studies in high carbon density mangrove ecosystems. In the tallest mangrove forest on Earth (Pongara National Park, Gabon), we leverage the data collected during the AfriSAR campaign to evaluate 17 state-of-the-art sensor data products across the full range of height and biomass known to exist globally in mangrove forest ecosystems, providing a much-needed baseline for sensor performance. Our major findings are: (Houghton, Hall, Goetz) height estimates are not consistent across products, with opposing trends in relative and absolute errors, highlighting the need for an adaptive approach to constraining height estimates (Panet al., 2011); radar height estimates had the lowest calibration error and bias, with further improvements using LiDAR fusion (Bonan, 2008); biomass variability and uncertainty strongly depends on forest stature, with variation across products increasing with canopy height, while relative biomass variation was highest in low-stature stands (Le Quéré et al., 2017); a remote sensing product's sensitivity to variations in canopy structure is more important than the absolute accuracy of height estimates (Mithardet al., 2014); locally-calibrated area-wide totals are more representative than generalized global biomass models for high-precision biomass estimates. The findings presented here provide critical baseline expectations for height and biomass predictions across the full range of mangrove forest stature, which can be directly applied to current (TanDEM-X, GEDI, ICESat-2) and future (NISAR, BIOMASS) global-scale forest monitoring missions.

1. Introduction

Forests hold approximately 45% of the world's active carbon

(Houghton, Hall, Goetz, Cohen et al., 2013, Bonan, 2008), sequestering approximately 32% of anthropogenic emissions every year (Le Quéré et al., 2017). Accurate estimates of the distribution and total

* Corresponding author. NASA Goddard Space Flight Center, Greenbelt, MD, USA.

E-mail address: atticus.stovall@nasa.gov (A.E.L. Stovall).

<https://doi.org/10.1016/j.srs.2021.100034>

Received 9 August 2021; Received in revised form 2 November 2021; Accepted 9 November 2021

Available online 13 November 2021

2666-0172/© 2021 Published by Elsevier B.V. This is an open access article under the CC BY-NC-ND license (<http://creativecommons.org/licenses/by-nc-nd/4.0/>).

carbon held in Earth's forests are essential for modelling and monitoring climate change, yet many global maps of carbon storage disagree in critical regions of high carbon density (Mitchard et al., 2014). Mangroves, in particular, have the highest total carbon density of any forest on Earth with a mean of 856 Mg ha⁻¹, 49–98% of which is stored in the first 3 m of soils (Donato et al., 2011), (Kauffman et al., 2020), with C burial rates of 226 ± 39 g C/m²/yr in comparison to 4 ± 0.5 g C/m²/yr in tropical terrestrial forests (McLeod et al., 2011). Total mangrove aboveground biomass (AGB) is estimated at 1.75 Pg (Simard et al.), with soil carbon measurements in the range of 1.93–6.4 Pg C (Ouyang, Lee), (Sander et al., 2018), yielding approximate total carbon estimates of 2.7–7.2 Pg C. Additionally, these forests provide valuable ecosystem services – fuel, construction materials, and protection from storms – to local coastal populations (Barbier, 2016), (Ewel et al., 1998) and essential habitat for rare and endangered animal species (Gopal and Chauhan, 2006). Despite their importance, anthropogenic-driven loss is occurring on a global scale (Thomas et al., 1996), (Goldberg et al., 2020). In the face of climate change, a detailed understanding of the spatial distribution of carbon storage across the landscape will make future conservation efforts more fruitful (Worthington et al.) and help countries attain Nationally Determined Contribution (NDC) emissions reduction targets over the next half century.

National-scale carbon inventories contrast in level of detail and uncertainty of estimates. The confidence in reported carbon stocks dictate the three IPCC tiers, corresponding to estimates from [i] Tier 1: a mean ecosystem carbon density, [ii] Tier 2: deploying height-stratified field plots for improved mean carbon density, or [iii] Tier 3: spatially continuous carbon estimates calibrated with field plots and modeled with remote sensing (2006Guideline, 2006). Global conservation and forest ecology is entering a “golden age” of satellite measurements that stands to significantly improve our current understanding of fine-scale patterns in forest structure and carbon storage (Lucas et al., 2017). Remote sensing is enabling near-universal Tier 3 carbon estimates, but the long list of mapping products have yet to be directly compared to one another and important sensor-specific differences in forest height and biomass have not been quantified.

Key missions designed specifically for measuring forest structure include NASA's Global Ecosystem Dynamics Investigation (GEDI), ESA's BIOMASS (Le Toan et al., 2018), and NASA-ISRO's Synthetic Aperture Radar (NISAR (Rosen et al., 2016)). GEDI - a large-footprint waveform LiDAR (Light Detection And Ranging) sensor - solves many of the greatest challenges for creating high-certainty global forest carbon maps (Dubayah et al.). To capture sub-kilometer variations in forest structure, sampling instruments like GEDI or ICESat-2 (dense photon counting LiDAR) must be matched to contiguous height estimates – from either optical or, preferably, radar (Qi and Dubayah, 2016). DLR's TerraSAR-X add-on for Digital Elevation Measurement (TanDEM-X or TDx) DEM product provides a ~12 m resolution digital surface model (DSM) at a global scale, making it ideal for creating high-resolution spatially continuous forest height products (Krieger et al., 2007), (Lee et al., 2018). In tropical forests, upcoming SAR sensors like BIOMASS (P-band) and NISAR (L-band) can penetrate cloud cover, enabling detailed estimates of forest structure that are unreachable with optical and LiDAR remote sensing alone (Mitchard et al., 2012). However, radar backscatter loses sensitivity at high biomass densities - highlighting the need for more direct estimates of structure from SAR (i.e. InSAR) together with multi-faceted fusion approaches as the most viable option for globally consistent estimates of forest structure. In mangroves specifically, Simard et al. (Simard et al.) created a global high-resolution mangrove height and biomass maps using Shuttle Radar Topography Mission (SRTM) data calibrated with NASA Ice, Cloud, and land Elevation Satellite (ICESat) Geoscience Laser Altimeter System (GLAS) and forest inventory data. However, these maps represent the status of global mangrove forest in the year 2000 with 30-m spatial resolution and limited accuracy at local scales. Given the wealth of current and upcoming near-global remote sensing data capable of estimating forest

height and biomass, there is a clear need to evaluate the consistency and differences across sensors in the context of height and biomass.

In this study, we evaluate 17 forest biomass products from five types of sensors measuring canopy structure ([i] stereo optical photogrammetry, [ii] SAR interferometry, [iii] Polarimetric SAR interferometry, [iv] large-footprint waveform LiDAR and [v] photon counting LiDAR in the tallest known mangrove forest (Simard et al.), leveraging data collected from the 2016 AfriSAR airborne campaign as well as in situ measurements in Gabon (Fatoyinbo et al., 2017), (Fatoyinbo et al., 2021). These products were derived from airborne and spaceborne sensors representing the suite of current and future missions used for measuring forest height, estimating aboveground biomass and ecosystem carbon stocks. The specific objectives of this study are:

1. Directly compare remotely sensed height products;
2. Develop and evaluate sensor-specific biomass calibration models from plot data;
3. Directly compare spatial distributions of locally calibrated and other biomass products;
4. Directly compare area-wide totals from locally calibrated and other biomass products.

The goal of our analysis is to provide a baseline comparison of height and biomass estimates for the most commonly available airborne and spaceborne remote sensing products, providing a much-needed baseline for current and forthcoming sensor performance.

2. Methods – 2362

The analysis in this study used field inventory biomass estimates to calibrate a suite of remotely sensed height to generate spatially comprehensive maps of biomass over the study site. The height and biomass maps, and biomass totals are then intercompared.

2.1. Site description and field data

The study site is the Pongara National Park located in Gabon (Fig. 1). Pongara National Park is located on the southern bank of the Komo Estuary, directly south of Libreville, Gabon's capital city. The Park covers an area of 87,000 ha and is covered primarily by mangroves (52,700 ha) and some *terra firme* rainforests (Dauby et al., 2008). This site holds both the tallest known mangrove forests on Earth and large areas of short low density stands – an excellent test case for capturing a range in forest stature from 2 m to in excess of 60 m in height (Simard et al.).

Circular field plots (n = 17) were sampled with a radius between 6 and 12.5 m diameter, with small plots coinciding with short stature forest stands (Trettinet et al., 2020). At each plot, aboveground biomass (AGB) was estimated from stem diameter measurements (0.5 m above the last prop-root). In addition, tree height was estimated using a laser hypsometer. In this study, we chose to use height-based field allometry from Chave et al. (Chave et al., 2014)'s wet tropical equation as it best related to our remotely-sensed height estimates:

$$\text{Aboveground Biomass (kg)} = \exp(\alpha + \beta \ln(\rho D^2 H)) \quad [1]$$

Where α and β are model coefficients derived from least squares regression, ρ is species-specific wood density (0.9 for *Rhizophora* sp.), D is tree diameter, and H is tree height.

For reference and to determine the impact of allometric equation selection, we also evaluated the difference in plot-level biomass estimates using allometry relying solely on tree diameter (See Fig. S1, Table S1, and Fig. S2; (Komiya, Pongparn, Kato)).

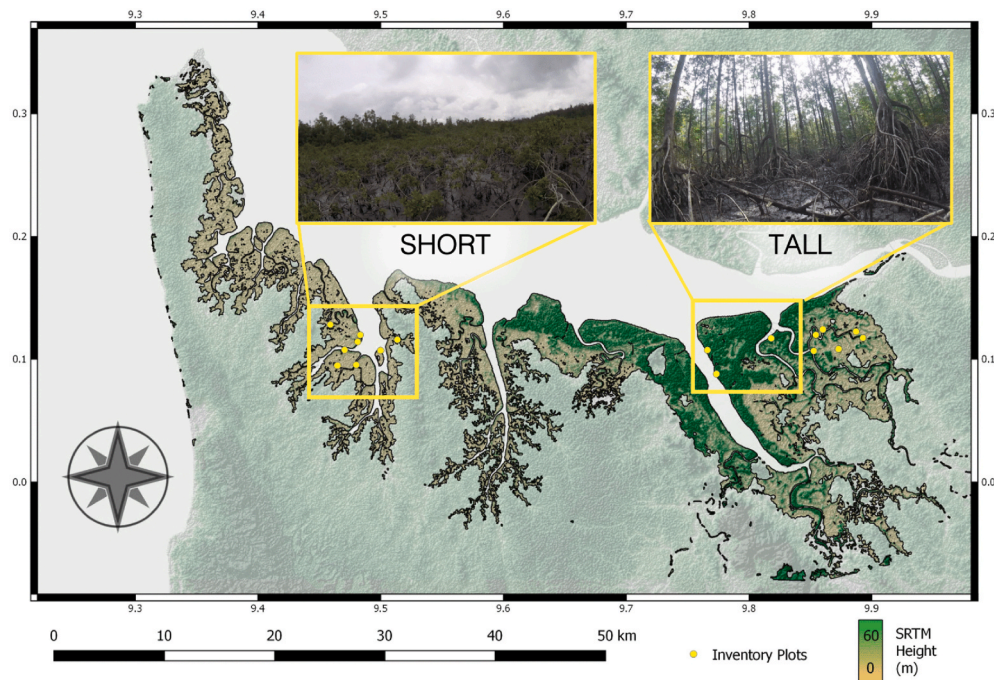


Fig. 1. Map of Pongara National Park with heights from SRTM-based global height product (from Simard et al. (Simard et al.)). Inventory plots were placed such that canopy heights were sampled proportionally according to the height distribution across the site.

2.2. Remote sensing datasets

We evaluated height and/or biomass products of global and local spatial extent (Fig. 2; Table 1). We evaluated five types of sensors measuring canopy structure using [i] stereo optical photogrammetry, [ii] SAR interferometry, [iii] Polarimetric SAR interferometry, [iv] large-footprint waveform LiDAR and [v] photon counting LiDAR. Specific details on products and processing techniques for individual products can be referenced from the associated publications in Table 1. Spatially continuous height products were not modified prior to biomass calibration to ensure the generalization of our analysis and results. Measurements from spaceborne LiDAR instruments –ICESat-2 and GEDI were used to calibrate TanDEM-X heights at the corresponding sensor resolution to produce two additional LiDAR-calibrated height and biomass map products.

2.2.1. Brief sensor overview

Several of the global sensor products evaluated here were produced in the 2000–2010 timeframe. The Advanced Land Observing Satellite (ALOS) Panchromatic Remote-sensing Instrument for Stereo Mapping (PRISM) is an optical instrument providing a 30 m stereo imagery-based digital surface model (DSM; (Tadono, Ishida, Oda, Naito, Minakawa, Iwamoto)), also referred to as a Digital Elevation Model (DEM). The Shuttle Radar Topography Mission (SRTM) was a C-Band SAR interferometry mission that flew in February 2000 producing a global ~30 m resolution Digital Surface Model (DSM). The SRTM DSM was used in concert with ICESat-1 (Ice, Cloud, and land Elevation Satellite (Zwally et al., 2002)); canopy height estimates to create local (Simard et al., 2008) and continental-scale (Fatoyinbo and Simard, 2013) and, more recently, the first global-scale (Simard et al.) canopy height and biomass models for mangrove forests. TanDEM-X is a high-resolution interferometric SAR mission launched by DLR (German Aerospace Center) to produce ~12 m (commercially available), ~30 m, and ~90 m (freely available) resolution global DSMs (Krieger et al., 2007).

We evaluated two recently launched global LiDAR sensors for measuring vegetation structure. The ICESat-2 satellite uses a photon-counting LiDAR to measure elevations (Abdlatiet al., 2010),

producing 100 m granule with vegetation indices. The low sampling density and polar orbit of ICESat-2 prevents evaluation of a continuous gridded height product. We therefore created continuous ICESat-2 mean canopy height product by calibrating 90 m TanDEM-X heights with 100 m ICESat-2 mean canopy height granules using a simple least squares regression model. The Global Ecosystem Dynamics Investigation (GEDI) instrument is a full-waveform LiDAR designed specifically to measure forest structure at a near-global scale using four high-powered (power) and four-low powered (coverage) beams (Dubayah et al.). Aboard the International Space Station (ISS), GEDI produces vegetation metrics at the footprint-level (~25 m) with high vertical resolution. Similar to ICESat-2, we created a continuous GEDI RH100 height product by calibrating 30 m TanDEM-X heights with footprint-level GEDI RH100 heights using a least squares regression model. Geolocation errors are common in the version 001 release of GEDI data and erroneous height measurements often occur in edge areas. A recent simulation study found that the expected GEDI geolocation error of 10 m may introduce more than 50% uncertainty into the resulting height estimates (Roy, Kashongwe, Armston). We therefore flagged and removed GEDI shots within 40 m of the forest edge to avoid potential mixed or non-mangrove footprints resulting from geolocation error.

Local scale sensors in this study were flown as part of the AfriSAR, a joint NASA and ESA (European Space Agency) airborne campaign (Fatoyinbo et al., 2017), (Fatoyinbo et al., 2021). The goal of the mission was to fly overlapping airborne sensors analogous to future missions (e.g. ESA BIOMASS (Le Toan et al., 2850), NASA-ISRO Synthetic Aperture Radar (NISAR (Rosen et al., 2016)); and GEDI) to measure forest structure. DLR deployed the airborne F-SAR - a dual band Pol-InSAR instrument analogous to NISAR (L-band) and BIOMASS (P-band) - and covered a small portion of the study area and field plots. JPL's UAVSAR, an L-band SAR covered nearly the entirety of Pongara National Park (Denbina et al., 2018). The Land Vegetation Ice Sensor (LVIS; (Blair, Rabine, Hofton)) has near-identical technology as GEDI, though with nearly continuous sampling, providing ~25 m footprints of full-waveform LiDAR measurements.

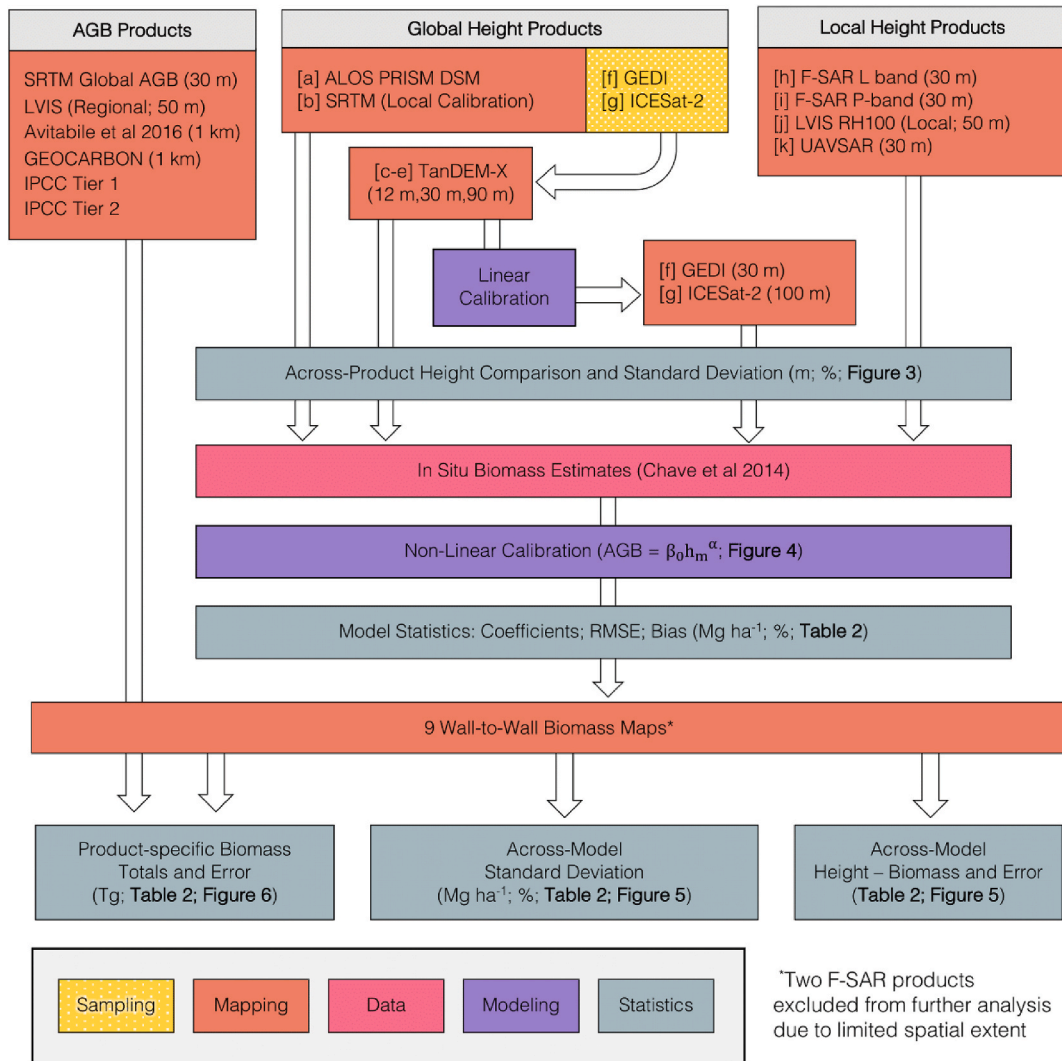


Fig. 2. Workflow detailing major processing and analysis steps used to compare 17 area-wide biomass products in Pongara National Park.

2.2.2. ICESat-2- and GEDI-TanDEM-X fusion

ICESat-2- and GEDI heights were used to calibrate two continuous TanDEM-X canopy height maps covering the entirety of the study area. For both spaceborne LiDAR sensors, we calibrated TanDEM-X heights with a similar procedure: [i] directly matching LiDAR heights to TanDEM-X heights, [ii] developing a calibration model between LiDAR height and TanDEM-X height, and [iii] producing a LiDAR corrected continuous height product covering the entirety of Pongara National Park.

All available overlapping ICESat-2 data were extracted for the study area comprising 46 total orbits of ATL08 data. All orbits were constrained to the study area and only those classified as mangrove were retained, leaving a total of 597 at 100 m intervals. We used the *h_{mean canopy}* variable in our calibration procedure – the mean of canopy heights within a 100 m granule. We used the 90 m TanDEM-X geoid-corrected height product (Simard et al.) to upscale ICESat-2 measurements since the two were closely matched in spatial scale. Next we extracted the 90 m resolution TanDEM-X heights at the overlapping ICESat-2 granules. In an initial assessment between the two heights, we found beam three had consistently anomalous height estimates; We therefore excluded data from this beam entirely. We identified and removed two extreme outliers in the calibration, based on the values exceeding 10× the mean Cooks Distance in the linear model. In total, we built the calibration model on 391 ICESat-2 height measurements.

Similarly, all available overlapping GEDI data was extracted for the study area – 21 total orbits of L2B data. Again, all orbits were constrained to the study area, retaining only mangrove areas and quality flag 1 data, leaving a total of 3482 canopy height estimates. We used the *rh100* variable in our calibration procedure – the tallest detectable height aboveground.

As expected, the two height variables for both ICESat-2 and GEDI data were closely and linearly related, so we used a least squares regression to develop the calibration model:

$$ICESat2 \text{ or } GEDI \text{ Canopy Height } (m) = \beta_0 + \beta_1 h_{TDX}$$

Where β_0 and β_1 are model coefficients and h_{TDX} is 90 m resolution geoid corrected TanDEM-X height.

2.3. Height and biomass analysis

The aim of our analysis was to compare the current available airborne and spaceborne remote sensing products for estimating forest height and biomass (Fig. 2). Both analyses of height and biomass compared each individual remote sensing product to a mean map (and standard deviation) created from all products. We evaluated the deviation of each product height and biomass from the mean with residual plots. Finally, we compared the total estimated biomass (and uncertainty) across the study site from each remote sensing product, along

Table 1
Specifications of sensors and products used for local calibration and/or validation in the study.

Extent	Sensor/Product	Product Resolution	Technology	Acquisition Period	Availability	Variable ^a	Relevant Publications
Global Height Products	[a] ALOS PRISM DEM	30 m	Stereo Optical	Jan 24, 2006–Apr. 22, 2011	Open	Elevation	(Tadono, Ishida, Oda, Naito, Minakawa, Iwamoto)
	[b] SRTM	30 m	C-Band SAR Interferometry	Feb 11–22, 2000	Open	Ice-SAT-GLAS-Corrected Mangrove Canopy Height (Hmax)	(Simard et al.), (Farret al., 2007)
	[c] TanDEM-X (12 m)	12 m	X-Band SAR Interferometry	Dec 12, 2010–Jan 16, 2015	Commercial	Geoid corrected height asl	Krieger et al. (2013)
	[d] TanDEM-X (30 m)	30 m			Commercial		
	[e] TanDEM-X (90 m)	90 m			Open		
	[f] ICESat-2-TanDEM-X	100 m	Photon Counting LiDAR	Sept 15, 2018 - Present	Open	TanDEM-X Elevation corrected with ATL08 98th percentile heights	(Farret al., 2007), (Krieger et al., 2013)
	[g] GEDI-TanDEM-X	30 m	Large-Footprint Full-Waveform Spaceborne LiDAR	Mar 25, 2019 - Present	Open	TanDEM-X Elevation corrected with RH100 heights	(Dubayah et al.)
Local Height Products	[h] LVIS	50 m	Large-Footprint Full-Waveform Airborne LiDAR	Mar 3, 2016	Open	RH100	(Blair, Rabine, Hofton)
	[i] F-SAR L band ^c	30 m	Airborne L-Band PolinSAR	Feb 2016	Open	Modeled Canopy Height	(Pardini et al., 2018), (Horn et al., 2009)
	[j] F-SAR P-band ^c	30 m	Airborne P-Band PolinSAR	Feb 2016	Open	Modeled Canopy Height	(Pardini et al., 2018), (Horn et al., 2009)
	[k] UAVSAR	30 m	Airborne L-Band PolinSAR	Feb 27, 2016	Open	Modeled Canopy Height	Hensley et al. (2008)
AGB products	LVIS (Regional Calibration)	50 m	Large-Footprint Full-Waveform Airborne LiDAR	Mar 3, 2016	Open	AGBD ^b	(Horn et al., 2009), ^b (Hensley et al., 2008)
	Global SRTM	30 m	C-Band SAR Interferometry	Feb 11–22, 2000	Open	AGBD ^b	^b (Simard et al.), (Fatoyinbo and Simard, 2013)
	Avitabile et al. 2016 GEOCARBON	~1 km	SAR, Optical, Large Footprint LiDAR	2011–2012	Open	AGBD ^b	^b (Saatchi et al., 2019), ^b (Armstrong et al., 2020)
	IPCC Tier 1 value: 192 Mg ha ⁻¹ IPCC Tier 2 value: 215 Mg ha ⁻¹	–	–	Mar 2016	–	IPCC mean mangrove AGBD Plot-based	^b (2006Guideline, 2006)

^a The predictor variable matched to plot data used for calibrating the allometric models of aboveground biomass.

^b Aboveground biomass density estimates derived in the cited study.

^c Height-biomass calibration is only evaluated due to limited spatial extent.

with six other external AGB maps and IPCC Tier 1 and Tier 2 AGB estimates. In doing so, we provide a basis for comparison and a baseline expectation for height and biomass estimates for all products analyzed in this study.

2.3.1. Evaluating remotely sensed mangrove height

Height estimates from nine height products were intercompared at the pixel level over their mutually overlapping area. To evaluate the variability across all height products ($H_{product}$), we calculated the per-pixel (i) average ($mean$) and standard deviation (sd) of all height maps to create a single map representing the mean height (H_{mean}) and standard deviation (H_{sd}) of height:

$$H_{mean}(i) = mean(H_{product}(i)) \quad [2]$$

$$H_{sd}(i) = sd(H_{product}(i) - H_{mean}(i)) \quad [3]$$

We evaluated the overall trend in standard deviation from Eq. (3) with respect to 1 m bins of H_{mean} . For individual continuous AGB products ($AGB_{product}$; $n = 9$) by calculating the mean signed deviation (MSD) and standard deviation (H_{sd}) as a function of 1 m bins of H_{mean} , represented as h in equations (4) and (5):

$$MSD(h) = mean(H_{product}(i, h) - H_{mean}(i, h)) \quad [4]$$

$$H_{sd}(h) = sd(H_{product}(i, h) - H_{mean}(i, h)) \quad [5]$$

We also determined how well specific products capture field-measured heights (based on RMSE and bias) by directly comparing the remotely sensed heights to plot-level tree height percentiles.

2.3.2. Sensor aboveground biomass calibration and uncertainty

For each of the remote sensing height products, we built a calibration model relating in-situ plot biomass to remotely sensed height using non-linear least squares regression (nls ; R Core Team 2019) with the form:

$$Aboveground\ Biomass\ (Mg\ ha^{-1}) = \beta_0 h_m^\alpha \quad [5]$$

Where β_0 is the scaling coefficient, h_m is a sensor-specific height metric, and α is the scaling exponent. Note, none of the remote sensing products we evaluated had a resolution smaller than the plot size (6–12.5 m diameter), so the value of h_m was simply extracted at the plot location. However, plots were established in ~0.5 ha areas of homogeneous height to mitigate the effects of the smaller plot size (See Trettin et al. (Trettin et al., 2021) for details), making the plot data representative for resolutions up to ~70 m. In addition, we used this same model form to evaluate a purely plot-based allometric model (see [Supplementary Material Fig. S1](#)).

The precision and accuracy of all locally calibrated predictive

biomass models were assessed with a bootstrapped estimate of root mean square error (RMSE) and bias. Over 1000 iterations, a random set of 70% of the plot data was selected for model training using Equation (2). The predicted value was then compared against the independent (measured) plot biomass values using the following equations:

$$RMSE (Mg\ ha^{-1}) = \sqrt{\frac{\sum_{i=1}^n (predicted_i - measured_i)^2}{n}} \quad [6]$$

$$RMSE (\%) = \frac{RMSE}{\overline{measured}} \quad [7]$$

$$Bias (Mg\ ha^{-1}) = \frac{\sum_{i=1}^n predicted_i - measured_i}{n} \quad [8]$$

$$Bias (\%) = \frac{Bias}{\overline{measured}} \quad [9]$$

Where $\overline{measured}$ is the mean plot-level biomass density estimate across all iterations. In an additional analysis, we evaluated the role of model uncertainty in calibration coefficient estimates. A robust parameter-based non-linear pixel-level error estimate for each biomass product was estimated directly from the non-linear calibration models using the first-order Taylor series method as implemented in the *errors* package in R (Language, 2019), (Ucar et al., 2019). In essence, this method linearizes the predicted biomass uncertainty for a given height, accounting for the variance and covariance between model coefficients (See documentation for *errors* package for further details). The approach simply uses the uncertainty in the calibration model parameters to properly estimate pixel-level prediction error.

2.3.4. Spatial patterns and variability in biomass

As in our height analysis (Section 2.3.1), AGB estimates from all spatially continuous height products were directly compared at the pixel level (excluding pixels with missing values from any sensor). To evaluate the variability across all height products ($AGB_{product}$), we calculated the per-pixel average and standard deviation of all AGB maps to create a single map representing the mean AGB (AGB_{mean}) and standard deviation (AGB_{sd}) of height:

$$AGB_{mean}(i) = mean(AGB_{product}(i)) \quad [10]$$

$$AGB_{sd}(i) = sd(AGB_{product}(i) - AGB_{mean}(i)) \quad [11]$$

We evaluated the overall trend in standard deviation with respect to 10 Mg ha⁻¹ bins of AGB_{mean} . For individual continuous height products ($AGB_{product}$; $n = 9$), we calculated the mean signed deviation (*MSD*) and standard deviation (AGB_{sd}) as a function of 10 Mg ha⁻¹ bins of AGB_{mean} , represented as b in equations (4) and (5):

$$MSD(b) = mean(AGB_{product}(i, b) - AGB_{mean}(i, b)) \quad [12]$$

$$AGB_{sd}(b) = sd(AGB_{product}(i, b) - AGB_{mean}(i, b)) \quad [13]$$

In addition, we compared the mean biomass predictions (AGB_{mean}) of our area-wide locally calibrated estimates on a per-pixel basis to two contrasting high-resolution independent biomass products based on SRTM (30 m; (Simardet al.)) and LVIS (50 m (Armstonet al., 2020)). We quantified systematic deviations, highlighting these differences using residual variation figures.

2.3.4. Total biomass and uncertainty

Total biomass and uncertainty was estimated across the entire study area for all continuous remote sensing biomass products – nine locally calibrated models and six baseline biomass estimates (Fig. 2). For the nine locally-calibrated biomass products, we limited the spatial extent to that of the product with lowest spatial coverage (i.e. LVIS). Across this area, we derived the mean biomass prediction and associated

uncertainty (determined with pixel-level model parameter-based first-order Taylor series method). The mean and uncertainty estimates were applied across the ~40,000 ha study area for area-wide biomass totals. Uncertainty was propagated using the *errors* package in R (Language, 2019), (Ucar et al., 2019).

We evaluated the totals from six baseline biomass estimates described in Table 1: [i] Global SRTM mangrove biomass (Simardet al.), [ii] regionally calibrated three-variable LVIS biomass (Armstonet al., 2020), [iii] Avitabile et al. (Avitabileet al., 2016), [iv] Santoro et al. (Santoroet al., 2015) global biomass products (1 km), [v] IPCC Tier 1 values (192 Mg.ha-1), and [vi] IPCC Tier 2 (215 Mg ha⁻¹). The global SRTM mangrove biomass product is based on globally calibrated ICESat-GLAS adjusted SRTM heights (H_{max} variable, (Simardet al.)). The regional LVIS biomass product was calibrated from all other non-mangrove field data included in the Gabon AfriSAR campaign (see (Armstonet al., 2020)). The Avitabile et al. (Avitabileet al., 2016) and Santoro et al. (Santoroet al., 2015) global biomass products are built from a suite of active and passive remote sensing variables covering the pantropical and global scale, but are not specifically calibrated for mangroves. To ensure our area-wide totals were not biased by product coverage, we limited the extent of each continuous mapped product to the study area, calculated the mean mangrove biomass density estimate of all pixels, and applied the mean values to the entirety of Pongara National Park. For comparison, we included Tier 1 and Tier 2 IPCC-based biomass estimates in our total biomass and assessment. The Tier 1 IPCC estimate was based on the Mangrove Tropical Wet area-based mean (192 Mg ha⁻¹). The field plots were established using probability-based sampling, so for comparison we also derived a Tier 2 IPCC estimate calculated as the mean plot-based biomass (215 Mg ha⁻¹). Both Tier 1 and 2 mean values are not spatially explicit and were simply applied to the total mangrove area used in this study. To ensure a consistent estimate of product uncertainty, baseline product uncertainty was estimated as the standard deviation of the difference between *in-situ* plot biomass and the mapped biomass estimate.

3. Results – 915

3.1. ICESat-2- and GEDI-TanDEM-X fusion

The ICESat-2 and GEDI height estimates successfully calibrated TanDEM-X heights ($R^2 = 0.84-0.93$). Table S2 provides an overview of the statistics of the final calibration models and Fig. 3 shows the calibration models, along with anomalous excluded data. The ICESat-2 calibration had an order of magnitude fewer measurements available than GEDI, reducing the power of the calibration model. The ICESat-2 calibration model reduced TanDEM-X heights, while GEDI RH100 calibration increased TanDEM-X heights. The major factor affecting the quality of GEDI height estimates was the ground elevation estimate, which was used as criteria for data quality filtering.

3.2. Evaluating remotely sensed mangrove height

Height estimates from nine products were compared to the field height measurements and the mean height map (H_{mean}). Different aspects of canopy height are captured, depending on sensor (Fig. 4). TanDEM-X products generally underestimate, LVIS closely estimates, and the SRTM H_{max} product overestimates compared to field height. The ALOS PRISM DEM was highly variable and generally underestimated field height.

Most products generally followed a linear trend with the mean height map (H_{mean}) (Fig. 5, Fig. S4A). ALOS PRISM product had the lowest and SRTM H_{max} had the tallest height estimates covering ~25 m difference in the tallest stature stands, with TanDEM-X-based estimates clustering towards H_{mean} . UAVSAR had the only clear non-linear trend, with a saturating relationship above 20–30 m in mean height. Variability across all sensors increased non-linearly with mangrove stature (Figs. 5B

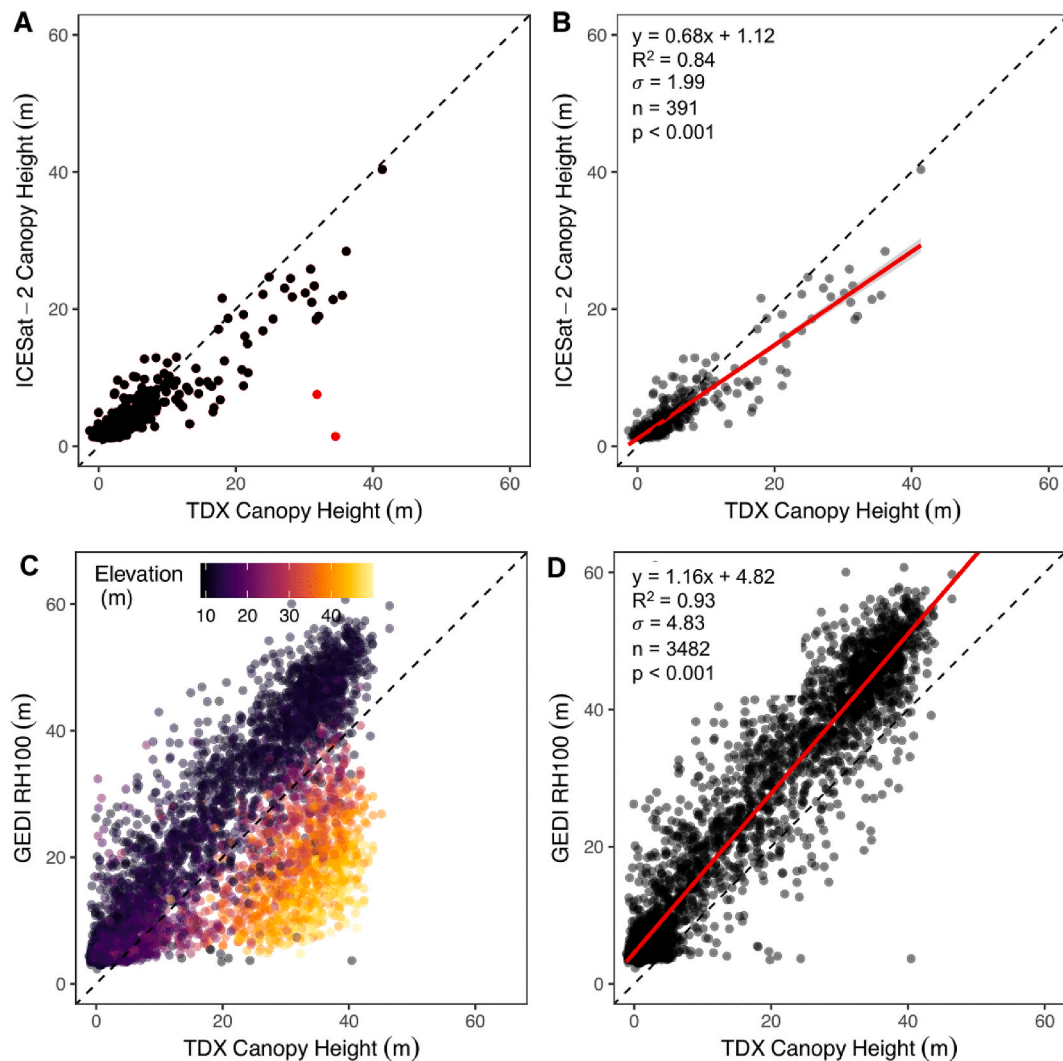


Fig. 3. Calibration models used to create spatially continuous height estimates by fusing ICESat-2 mean canopy height and GEDI RH100 to TanDEM-X continuous heights. Red points are removed outliers in the ICESat-2 calibration (anomalous beam 3 data not shown). Colored points in C show anomalous elevation values that were removed from the final calibration model (B and D). (For interpretation of the references to color in this figure legend, the reader is referred to the Web version of this article.)

and 3D) to a maximum of ~ 8 m. Variability of individual products with respect to height class displayed a peak of ~ 2.5 – 7 m at ~ 30 m H_{mean} after which remained constant or decreased slightly (Supplementary Material; Fig. S3; Fig. S4). Relative variation (%; H_{sd} normalized by H_{mean}) universally decreased with increasing H_{mean} (Supplementary Material, Fig. S4).

3.3. Sensor aboveground biomass calibration and uncertainty

Calibration models scaling coefficients ranged from 0.85 (SRTM H_{max} and ALOS PRISM Stereo DEM) to 3.11 (UAVSAR L-band height), with lower scaling coefficients generally having higher calibration uncertainty (Fig. 6; Table 2). The locally calibrated AGB products fell into two broad categories: [i] global spaceborne and [ii] local airborne sensors. AGB of spaceborne sensors had higher RMSE (mean = 78%, sd = 14%) than airborne sensors (mean = 62%, sd = 27%). Biomass models using airborne products were $\sim 5\%$ less biased than global spaceborne products. The best performing models for local and global height products were PolInSAR (L-band F-SAR; RMSE = 121 Mg ha^{-1} ; P-band F-SAR; RMSE = 71 Mg ha^{-1} ; UAVSAR; RMSE = 92 Mg ha^{-1}) and X-band interferometry (TanDEM-X; RMSE = 142 Mg ha^{-1}), respectively. The GEDI calibrated TanDEM-X AGB product had lower uncertainty than the

TanDEM-X AGB product of the equivalent spatial resolution (RMSE = 139 Mg ha^{-1} ; 146 Mg ha^{-1}). ICESat-2 calibration of TanDEM-X heights did not improve model performance (RMSE = 180 Mg ha^{-1}). The F-SAR products covered only 4–5 of the field plots and 20% of the study area, altering mean plot biomass (238 – 277 Mg ha^{-1} ; $\sim 50 \text{ Mg ha}^{-1}$ higher than other height products), but, while heights were lower than H_{mean} (Fig. S7), AGB predictions remained similar to AGB_{mean} (Fig. S8). Given the fact that LiDAR is considered one of the best means of creating areawide biomass maps, the large-footprint waveform LiDAR (LVIS RH100) had a higher than expected RMSE (174 Mg ha^{-1}), putting it on-par with other global spaceborne sensors (e.g. C-band SAR interferometry (SRTM; 190 Mg ha^{-1}) and stereo photogrammetry (ALOS PRISM DEM; 220 Mg ha^{-1})).

3.4. Spatial patterns and variability in biomass

Nearly all AGB products approximated AGB_{mean} with $\sim 60 \text{ Mg ha}^{-1}$ maximum standard deviation across all models above 600 Mg ha^{-1} (~ 30 m H_{mean} ; grey, Fig. 7). All TanDEM-X products clustered towards the AGB_{mean} , with ICESat-2 and GEDI estimate increasing AGB above 400 Mg ha^{-1} AGB_{mean} . The ALOS DEM AGB product was lower than average above 200 Mg ha^{-1} , while SRTM H_{max} AGB was higher than

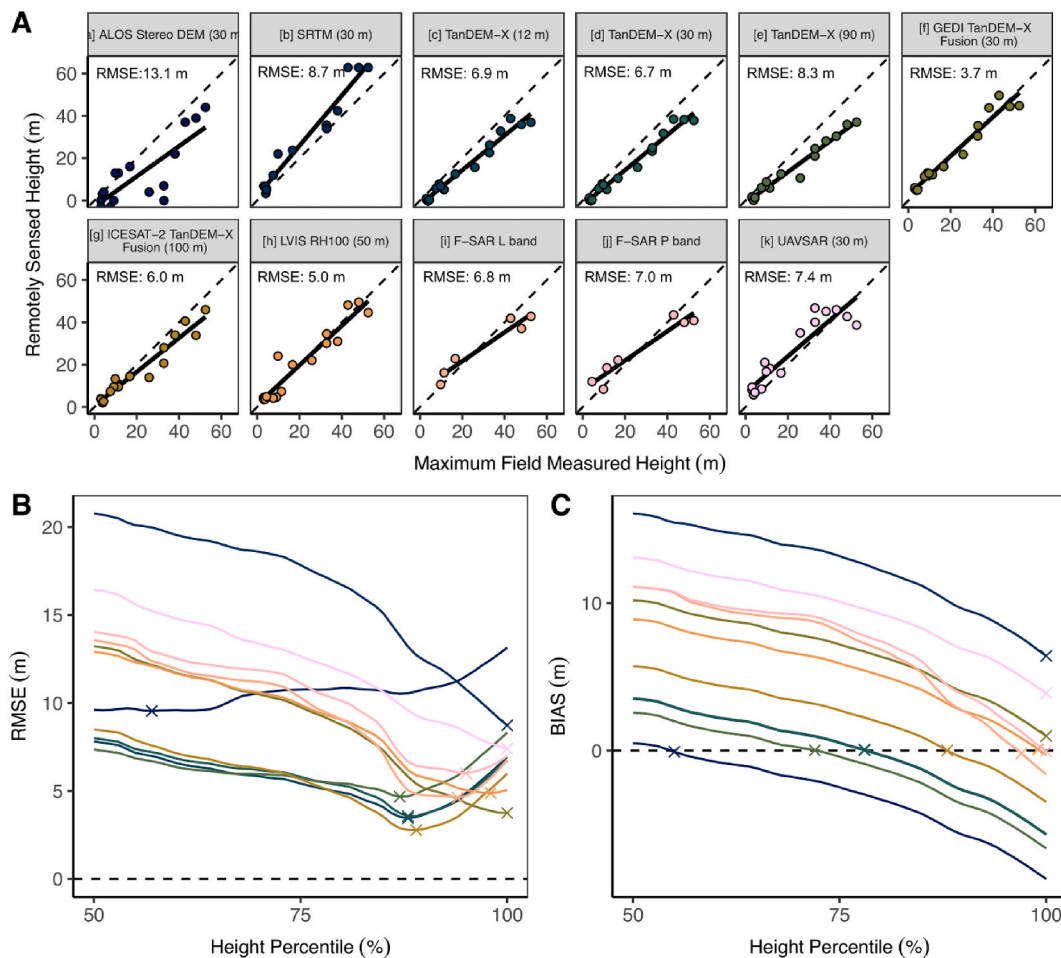


Fig. 4. [A] Comparison between maximum field measured height and remotely sensed heights (RMSE shown). Several remote sensing products estimate maximum field measured height, while some represent a specific percentile of field measured tree height. [B] RMSE and [C] bias in the comparison between field tree height percentiles (50th to 100th) and each remote sensing product. Colors correspond to point color shown in panel A and X's indicate the percentile at which RMSE or bias are lowest. (For interpretation of the references to color in this figure legend, the reader is referred to the Web version of this article.)

average below 200 Mg ha^{-1} . UAVSAR AGB was highly variable, but predicted consistently higher than AGB_{mean} . AGB_{sd} increased with AGB_{mean} class for all AGB products (Fig. 7; Supplementary Material; Fig. S5; Fig. S6). The 30 m global SRTM mangrove biomass product was consistently $\sim 40\%$ higher than AGB_{mean} , while the regional LVIS AGB product was $\sim 200\text{--}400 \text{ Mg ha}^{-1}$ lower compared to AGB_{mean} (Fig. 8). Both of these trends are clear in the difference maps (SRTM AGB - AGB_{mean} and LVIS AGB - AGB_{mean} ; Fig. 8A and B).

3.5. Total biomass and uncertainty

We compared area-wide totals of nine different locally calibrated AGB products, along with four regional and globally calibrated AGB products, and two IPCC tier-based estimates (Table 2; Fig. 9). All biomass models calibrated with the local plot data predicted similar total biomass for the entirety of Pongara National Park (Fig. 9) using both global spaceborne (mean = 6.8 Tg , $sd = 1.1 \text{ Tg}$) and local airborne sensors (mean = 7.8 Tg , $sd = 0.8 \text{ Tg}$). The global SRTM-based biomass model predicted $\sim 29\%$ higher total biomass than the locally calibrated SRTM model. The regionally calibrated tropical forest 3-variable LVIS model predicted $\sim 41\%$ lower biomass than the single-variable RH100 model. The local mean predictions were $\sim 19\text{--}29\%$ higher than the two 1 km global biomass maps (Avitabile et al., 2016), (Santoriet al., 2015). The global models had total uncertainty of $1.1\text{--}1.4 \text{ Tg}$ or $\sim 18\text{--}21\%$, compared to the 14% total uncertainty in the UAVSAR AGB product. In contrast, the IPCC Tier 1 area-based estimates for Mangrove Tropical

Wet forests had 9.6 Tg or 137% total uncertainty and the total predicted biomass was 6.9 Tg . The IPCC Tier 2 estimates increased average biomass from in-situ plot data, resulting in an increase to 7.8 Tg total AGB. The IPCC estimates were less than 0.8 Tg (12%) difference from the average biomass predicted from all locally calibrated high-resolution biomass products.

4. Discussion – 3335

Few previous studies have compared canopy height products from airborne and satellite products for terrestrial and mangrove forests and those that have are limited in the number of datasets (Sexton et al., 2009)– (Lucaset al.). Recently, new satellite sensors were launched and new overlapping airborne campaigns occurred, collecting a wealth of spatial data. We evaluate the broad spectrum of state-of-the-art sensor data products across the full range of height and biomass known to exist globally in mangrove forest ecosystems, providing a much-needed baseline for sensor performance. Our major findings are as follows:

(Houghton, Hall, Goetz) height estimates are not consistent across products, with opposing trends in relative and absolute errors, highlighting the need for an adaptive approach to constraining height estimates, depending on forest stature; (Panet et al., 2011) radar products had the lowest calibration error and bias, with superior results from airborne instruments and improvements to spaceborne estimates with LiDAR fusion using height alone;

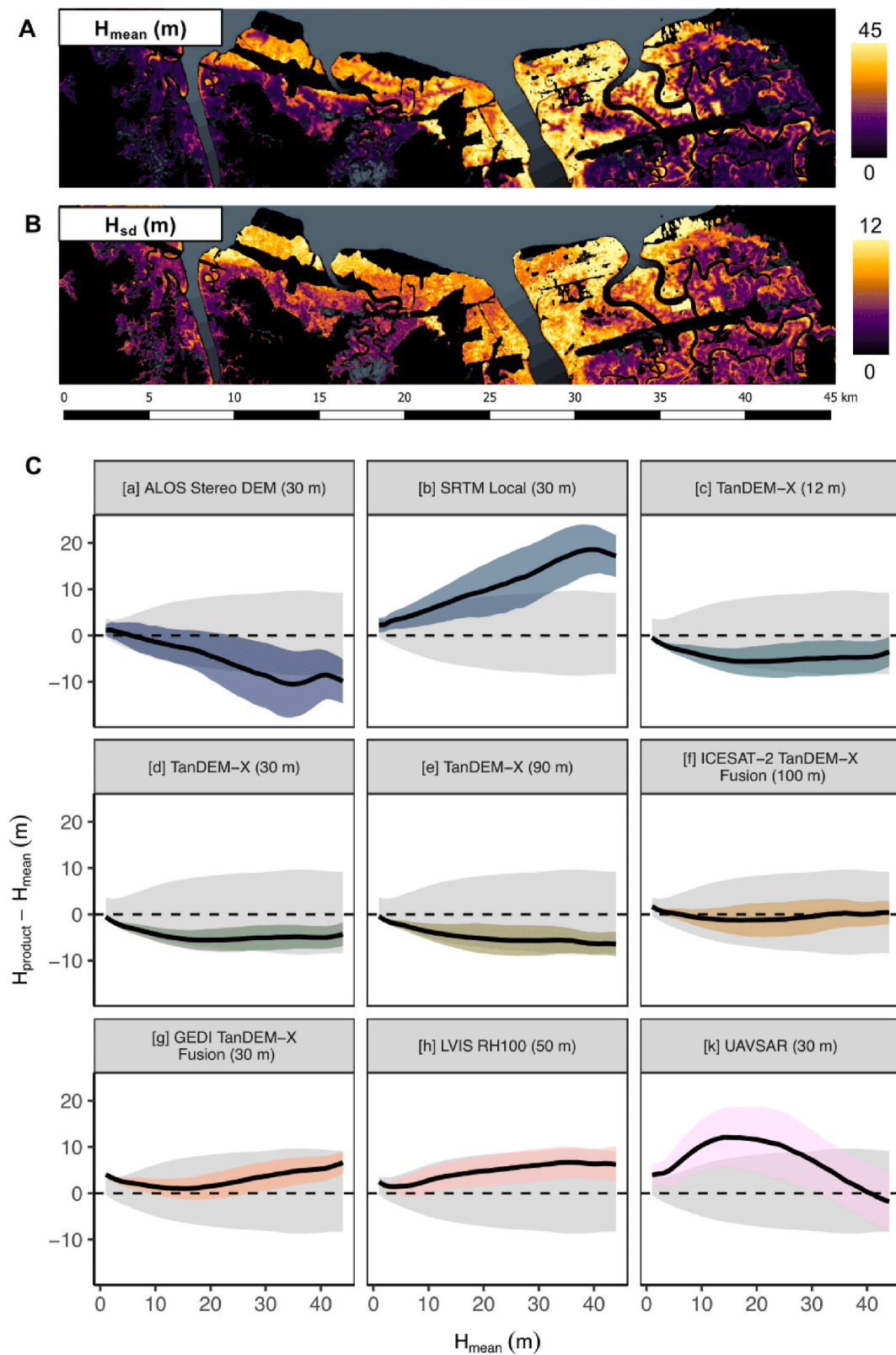


Fig. 5. (A) Example map of mean mangrove canopy height (H_{mean}) and (B) variation across the 9 sensors compared in this study. Relationship between sitewide mean mangrove canopy height (H_{mean}) and (C) product heights minus H_{mean} and standard deviation (within a product (color) and across products (grey)) from 9 remote sensing products. Variability increases with H_{mean} , while the equivalent relative variation decreases with H_{mean} (See [Supplementary Material Fig. S3](#)). (For interpretation of the references to color in this figure legend, the reader is referred to the Web version of this article.)

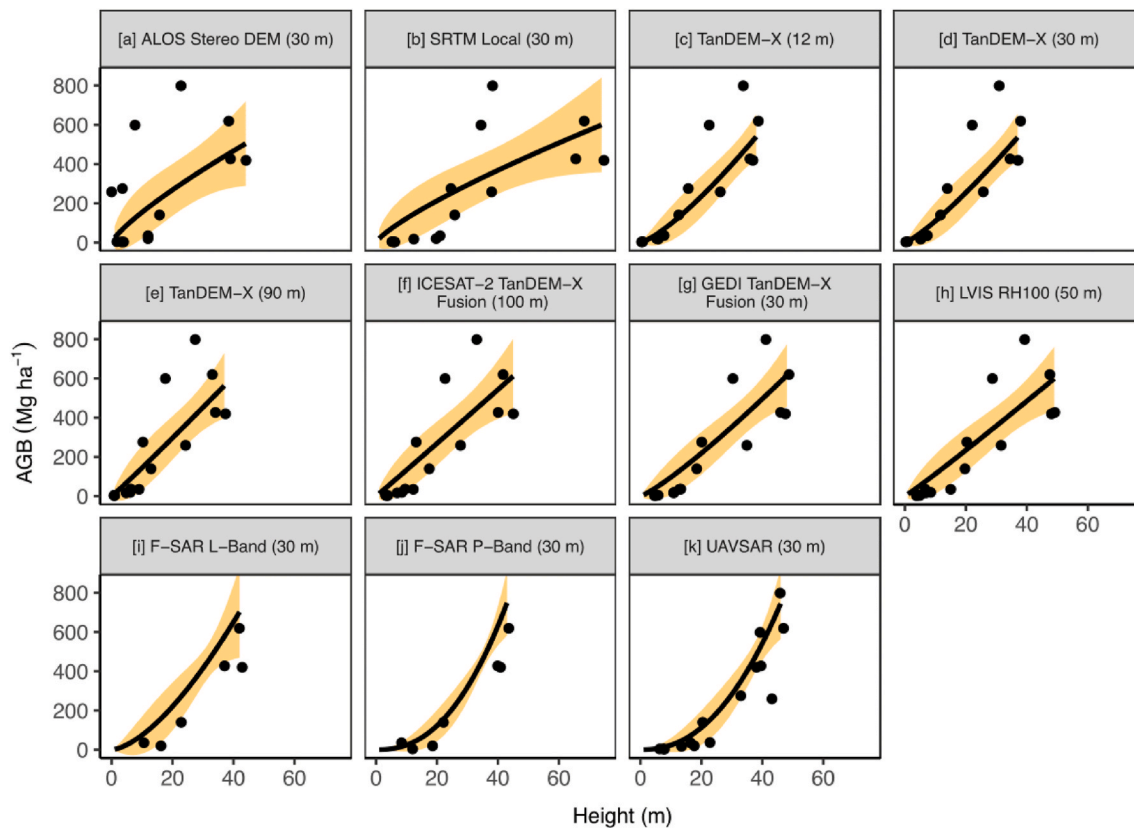


Fig. 6. Non-linear height allometry for 11 remote sensing products. See Table 2 for corresponding model coefficients and fit and validation statistics.

Table 2

Summary of comprehensive biomass calibration and predictions for the 17 products evaluated. All aboveground biomass (AGB) values are in $Mg\ ha^{-1}$ unless other units are specified. Uncertainty in the AGB prediction (σ) was derived from area-wide mean uncertainty from the AGB model parameter fits. Uncertainty in all baseline datasets was derived from an independent validation of the mapped values with the plot-level AGB estimates.

		Calibration				Validation				Totals				
		Mean AGB	Plots	β	α	RMSE	Bias	Bias (%)	RMSE (%)	Mean AGB	σ	Area (ha)	Total AGB (Tg)	σ
Global	[a] ALOS Stereo DEM (30 m)	215	17	20.21	0.85	220	7	3	102	178	57	34,960	6.4	2.1
	[b] SRTM Local (30 m)	226	16	15.89	0.85	190	18	8	84	232	59	37,870	8.4	2.1
	[c] TanDEM-X (12 m)	215	17	4.90	1.29	142	16	8	66	155	29	35,295	5.6	1.1
	[d] TanDEM-X (30 m)	215	17	6.47	1.21	146	21	10	68	156	30	36,350	5.6	1.1
	[e] TanDEM-X (90 m)	215	17	8.33	1.16	165	26	12	77	169	37	37,690	6.1	1.3
	[f] ICESAT-2 TanDEM-X Fusion (100 m)	215	17	9.20	1.11	180	26	12	84	205	45	37,771	7.4	1.6
	[g] GEDI TanDEM-X Fusion (30 m)	215	17	4.24	1.30	139	11	5	64	215	41	36,808	7.8	1.5
Local	[h] LVIS RH100 (50 m)	215	17	11.45	1.01	174	17	8	81	230	57	26,650	8.3	2.1
	[i] F-SAR L-Band (30 m)	277	6	2.05	1.56	121	16	6	44	408	50	7322	–	–
	[j] F-SAR P-Band (30 m)	238	7	0.10	2.37	71	–11	–5	30	368	33	7595	–	–
Baseline	[k] UAVSAR (30 m)	215	17	0.01	3.11	92	–5	–2	43	200	28	36,191	7.2	1.0
	SRTM Global (30 m)									301	90	31,491	10.9	3.3
	LVIS 3-Variable Regional (50 m)									136	36	26,864	4.9	1.3
	Avitabile et al., 2015 (1 km)									170	31	83,791	6.2	1.1
	GEOCARBON (1 km)									182	38	73,880	6.6	1.4
	IPCC Tier 1									192	264	–	6.9	9.6
	IPCC Tier 2									215	264	–	7.8	9.6

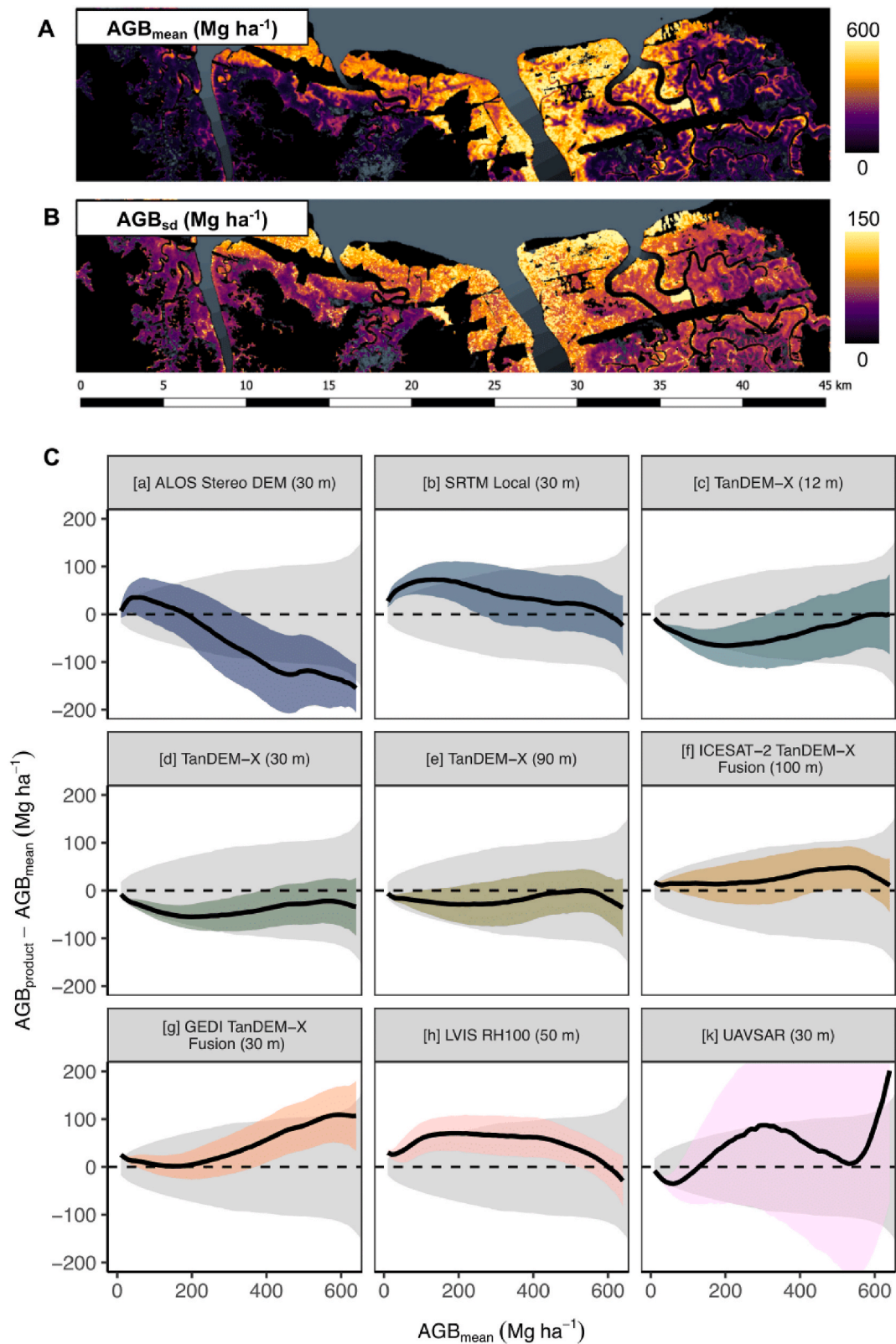


Fig. 7. (A) Example map of mean mangrove biomass (AGB_{mean}) and (B) variation across the 9 sensors compared in this study. Relationship between AGB_{mean} and (C) product biomass ($AGB_{product}$) minus AGB_{mean} (residuals), with standard deviation (within product (color) and across all products (grey)) from 9 remote sensing products. AGB variability increases with AGB_{mean} , while the equivalent relative variation decreases with AGB_{mean} (Supplementary Material, Fig. S5). (For interpretation of the references to color in this figure legend, the reader is referred to the Web version of this article.)

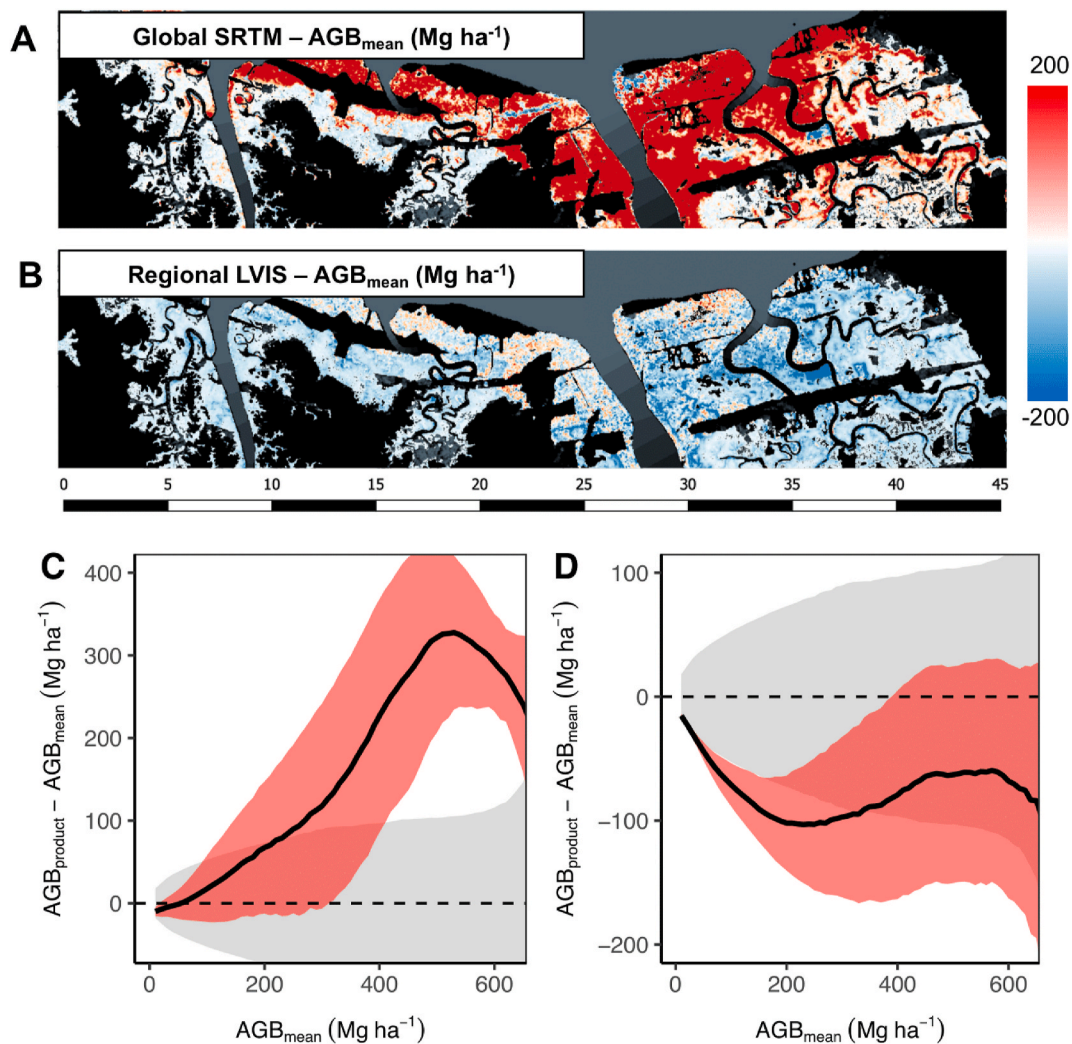


Fig. 8. Pixel-level comparison of local mean (across 9 products) aboveground biomass estimates (AGB_{mean}) and the [A] Global SRTM mangrove biomass and [B] regional LVIS biomass products. The residual plots indicate a systematic positive difference in the [C] SRTM-based model, increasing with increasing biomass values, and a systematic negative difference in the [D] regional LVIS biomass model.

(Bonan, 2008) AGB variability and uncertainty strongly depends on forest stature, with AGB_{sd} increasing with canopy height, while relative AGB_{sd} variation was highest in low-stature stands, suggesting the greatest improvements may be in low-to mid-biomass density ecosystems;

(Le Quéré et al., 2017) for AGB mapping, a remote sensing product's sensitivity to variations in canopy structure is more important than the absolute accuracy of height estimates;

(Mitchard et al., 2014) locally-calibrated area-wide totals are more representative than generalized global biomass models for high-precision biomass estimates;

Here, we first consider the more technical aspects of our results (Section 4.1) and follow with a discussion in the context of scientific and application-focused relevance at local, national, and global spatial scales (Section 4.2).

4.1. Evaluating remotely sensed forest height and biomass

4.1.1. Evaluating remotely sensed mangrove height

Mangrove canopy height estimates disagreed substantially across sensor type with absolute errors increasing as a function of canopy height. We attribute these differences almost universally to the sensor measurement approach capturing canopy height (Lagomasino,

Fatoyinbo, Lee, Feliciano, Trettin, Simard). An extreme example of the effect of measurement approach is with the ALOS PRISM product; Though past work highlighted the ALOS PRISM product as capable of capturing broad successional patterns in mangrove stands (Aslan et al., 2018), here, height estimates were insensitive to both low and tall stature forests compared to active remote sensing methods. Our comparison of remotely sensed height to plot-level height percentiles from tree-level inventory measurements highlights major differences in what part of the forest canopy is being measured with each height estimate (Fig. 3). InSAR instruments are simultaneously sensitive to height and vegetation volume density, which is preferable for biomass modeling. The existing SRTM H_{max} product is most representative of maximum tree height, but these estimates have high error (RMSE: $\sim 7-8$ m). The 12 m TanDEM-X phase center elevation product captures the 75th percentile of tree heights with 50% lower error than SRTM (RMSE: ~ 4 m) – potentially since TanDEM-X measurements were more closely temporally aligned to the field campaign (5 years vs. 17 years for SRTM). In both cases, field based validation of these remote sensing estimates is key to understanding the specific height attribute represented with a particular remote sensing product (Harding et al., 2001) and sensor choice should be dependent on the end goal (e.g. height vs. biomass).

Radar instrument wavelength and measurement technique reflected specific height anomalies. SRTM heights (C-band PolInSAR) differed positively from average with increasing canopy height, but height esti-

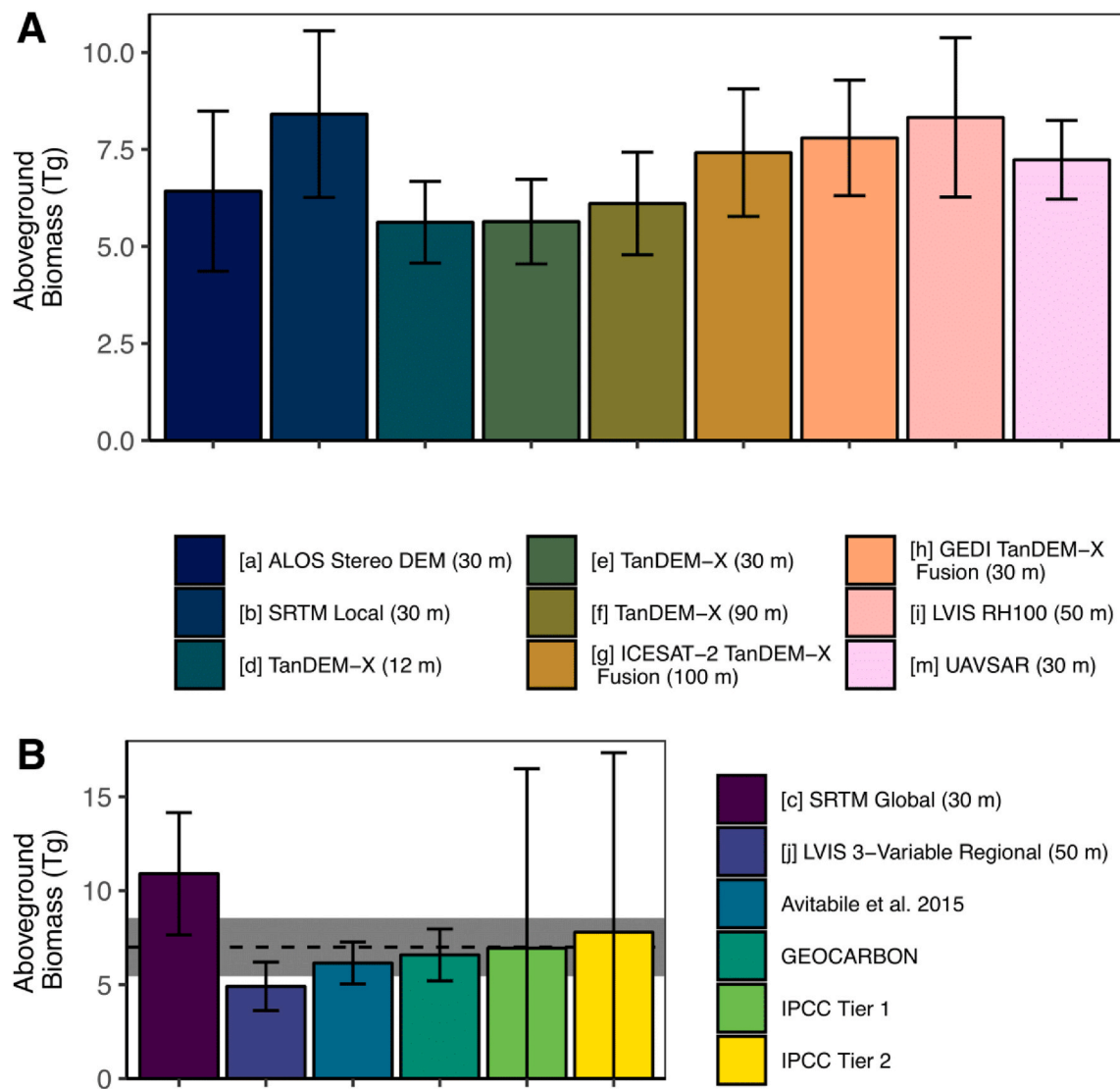


Fig. 9. Aboveground biomass totals for [A] nine locally calibrated and [B] six regional, global, and IPCC-based estimates. Totals are based on the mean estimates across the study area extrapolated via an area-based estimate. Error bars represent the 95% confidence interval of the total biomass estimate derived from plot based independent validation. Dotted black line and grey shaded area in B shows the mean and standard deviation of the locally calibrated area-wide biomass totals. Note: the y-axis scales between A and B are not fixed to highlight differences in each figure.

mates would be substantially underestimated without the ICESat GLAS-calibration and is likely affected by secondary structural variables (e.g. canopy cover or basal area). In agreement with past work (Denbina et al., 2018), UAVSAR (L-band) heights were consistent ($\sim \pm 10$ m average difference) until ~ 40 m height, above which heights became shorter than average – evidence of sensor saturation. TanDEM-X offers a precise, high-resolution height product that makes it one of the best options for continuous mapping of mangrove stands at a global scale. With the inclusion of additional height data (e.g ICESat-2 and GEDI), height estimates became less biased (up to 20 m offset in the tallest stands), pointing to a key fusion application in future studies. However, when calibrating continuous height products with sampling instruments, ground surface identification is a major issue in closed canopy systems and is likely exacerbated in the presence of water and dense aboveground mangrove root networks. All of these trends are consistent with our expectations of radar wavelength and forest height. In general, longer wavelengths penetrate further into the canopy, decreasing height estimates from the canopy top, but we expect height estimates are also influenced by canopy density.

4.1.2. Sensor aboveground biomass calibration and uncertainty

The height-biomass allometry across sensors varied from sublinear to linear with high uncertainty to more power-like models with low calibration uncertainty. In fact, we found a consistent negative trend between the scaling coefficient and model uncertainty. We also found a consistently higher mean biomass prediction with high-uncertainty models with lower scaling coefficient values – suggesting higher uncertainty models may be systematically over predicting biomass density (Simard et al.). Sensor measured height was the major factor affecting calibration uncertainty in our analysis, but other factors (e.g. plot size, plot shape, plot sample location, sample size, geolocation errors) can directly impact biomass calibration models and predictions. Future work in mangrove systems that independently evaluate these factors affecting model errors will provide more precise estimates of the spatial distribution of prediction uncertainty.

In general, radar sensors provided the lowest error and bias biomass calibration of the 11 local models, but the addition of LiDAR-derived canopy heights improved model statistics. InSAR (TanDEM-X) is likely the best available option for developing an updated global mangrove biomass product, evidenced by the low errors in calibration minimally

affected by product resolution (e.g. aggregating by a factor of 7.5 inflated RMSE by only 9%). The local scale L-band UAVSAR Polarimetric InSAR product performed even better, likely due to higher sensitivity to canopy cover, trunks and woody components (i.e. basal area). The higher than expected RMSE in the LVIS AGB model, suggests canopy height alone is a less powerful predictor than the phase center height captured with radar instruments. Radar-LiDAR fusion approaches (e.g. GEDI-corrected TanDEM-X heights) improve calibration by reducing bias and RMSE, but even greater benefits are possible in areas with greater topographic relief (e.g. non-mangrove systems), since LiDAR is primarily improving heights through more accurate ground detection. Though our intercomparison provides a robust analysis of height-biomass allometry for calibration of remote sensing datasets, we did not explicitly evaluate the suite of potential multi-variate approaches possible for predicting spatial distributions of AGB (e.g. (Armstrong et al., 2020)), especially for LiDAR sensors (e.g. GEDI, ICESat-2, and LVIS). As such, the results presented here do not emphasize the full benefits of using LiDAR-based multivariate models for biomass prediction. Future biomass calibration approaches should incorporate multivariate statistical approaches to take full advantage of the ability of LiDAR to capture internal canopy structure.

4.1.3. Spatial patterns and variability in biomass

Summarizing height-biomass trends from pixel-level predictions highlights the product-specific variations across AGB products in this tall mangrove system. Though plot based calibration models were often super-linear, site scale height-biomass allometry was more linear across all products, with AGB_{mean} increasing by 13 Mg ha^{-1} per unit H_{mean} . The most non-linear calibration model (UAVSAR) deviated most clearly from the general linear trend increasing more rapidly than AGB_{mean} from 0 to 25 m and increasing less rapidly above 25 m H_{mean} . The observed consistent linear relationship is ideal for cross-calibration, enabling more compatible multi-sensor approaches to biomass monitoring (Duncanson et al., 2020). Variability of a single AGB product was on the same order as the AGB variation across all products. Between 0 and 30 m, the standard deviation in mean biomass across all sensors increased linearly from 20 to 80 Mg ha^{-1} . Trends in pixel-level prediction uncertainty were similar for all sensors and within the range of AGB variation, increasing from 0 to 30, leveling off, then increasing to a maximum of $60\text{--}90 \text{ Mg ha}^{-1}$. Relative to traditional forest inventory methods, all locally calibrated remote sensing estimates had pixel-level uncertainty that was low, suggesting the use of a remote sensing framework is more important than the choice of sensor itself. For instance, the worst performing product calibration (ALOS PRISM; $RMSE = 102\%$) only translated to a marginal site-wide average uncertainty ($\sim 30\text{--}80 \text{ Mg ha}^{-1}$), suggesting a product's sensitivity to variations in canopy structure is more important than the absolute accuracy of height estimates.

Calibration of remote sensing products should be as local as possible in areas of high biomass density. Our comparison of the global SRTM biomass product to AGB_{mean} highlights the effects of generalized predictive models excluding representative plot data. The global product was systematically $\sim 40\%$ higher than the local predictions, resulting in more than 400 Mg ha^{-1} higher biomass density in some instances of high AGB_{mean} . While the Simard et al. (Simard et al.) map is unable to accurately capture biomass density in the high biomass areas of Pongara National Park, we believe the core cause is lack of calibration data in these extremely tall stands. Moreover, the map clearly provides the most accurate AGB predictions in mid-stature stands (10–20 m), where nearly all plot-level calibration data and global mangrove canopy heights reside. Alternatively, the regional LVIS AGB product is more precise, but is negatively biased, remaining within 100 Mg ha^{-1} throughout the AGB_{mean} range. The negative bias is similarly related to the product calibration, relying on lower mean wood density forest inventory data, pushing predictions lower than expected in Pongara, where *Rhizophora* sp. have ~ 0.9 specific gravity. We suggest establishing future field plots and planning airborne campaigns that fill data gaps in high-biomass

locations. For example, a targeted approach could use current AGB estimates to identify key areas of high AGB density with few or no available field data. Adding these additional *in-situ* observations will ultimately improve AGB calibration and provide more stable AGB predictions. In summary, these two global and regional products highlight the importance of appropriate plot-level calibration data to ensure both precise and accurate area-wide biomass distributions.

Two opposing patterns were clear with respect to variation in spatial biomass trends with forest stature: (Houghton, Hall, Goetz) absolute variation increases and (Panet et al., 2011) relative variation decreases. The extreme, tall forests have $\sim 200 \text{ Mg ha}^{-1}$ (or $\sim 20\%$) standard deviation on average across sensor predictions. Short forests (0–15 m) disagree by 40 Mg ha^{-1} (or $\sim 50\%$), on average. So, where will biomass model improvements be most impactful at the global scale: short or tall stands? We evaluated biomass models in a unique system capturing greater than 60 m of variation in mangrove forest structure, but more than 95% of the world's mangroves are less than 40 m tall (Simard et al.), suggesting the greatest benefits may be in low-to mid-biomass density ecosystems. Biomass is an essential biodiversity variable (Jetzet et al.), so improved biomass predictions stand to also directly affect biodiversity mapping and conservation efforts. These improvements will help to better capture changes in biomass over time in areas of growth, regeneration, degradation, and loss (Lagomasino et al., 2019). With this knowledge, we suggest developing global biomass products that are most precise in low-to mid-stature forests, but identifying and locally calibrating biomass models in tall-stature forests.

4.1.4. Total biomass and uncertainty

Locally calibrated biomass products provided similar total area-wide biomass estimates (all 95% confidence intervals overlap), even though biomass distributions often differed depending on sensor choice, having implications for carbon reporting and forest management. Accurate representations of the AGB distribution is key for identifying potential sites for restoration or conservation and carbon accounting priority (Worthington and Spalding, 2018), (Zeng et al., 2021).

Globally available biomass maps (Avitabile et al., 2016), (Santoro et al., 2015) performed well, underestimating total biomass by only $\sim 0.6 \text{ Tg}$ ($6.2\text{--}6.6 \text{ Tg}$ totals), with total uncertainty ranging from 18 to 20%. In contrast, compared to the mean AGB predicted with local models, the global SRTM model (Simard et al.) over predicted total biomass by $\sim 3.9 \text{ Tg}$ or 56%. The overprediction reflects two major issues: [i] the structure of this extremely tall mangrove stand is more closely analogous to a high wood density tropical forest than mangroves and [ii] inclusion of representative plot data is essential when building global biomass products (i.e. predictions outside of observations should be considered with caution).

From a carbon accounting perspective, the high uncertainty of these predictions substantially reduces their utility in tall forest stands, suggesting these global, coarse resolution generalized models should not be universally relied on for precise and accurate forest carbon estimates. The majority of mangrove calibration data resides in shorter stands (Simard et al.) and it is here where global biomass maps have less biased carbon estimates. Future global carbon maps should incorporate updated global height datasets that are freely available (e.g. TanDEM-X 90 m resolution), while also addressing the need for recalibration of past datasets as more calibration plot data becomes available. Surprisingly, the average area-based IPCC biomass density produced superior predictions, albeit not spatially explicit, limiting their utility for forest management and conservation.

4.2. Implications for multi-scale forest structure applications

4.1. Local scale

Mangrove forest height is uncertain across the products evaluated, posing a major challenge for incorporating remote sensing products into local forest management schemes. We found the relative uncertainty

across height products to be highest in low stature stands (>50% in stands <15 m), while in the tallest stands (~45 m H_{mean}) uncertainty was ~20% or 7–8 m. For context, many forest definitions rely on height thresholds of 5 or 10 m, so the uncertainty in these lower stature forests may impact estimates of forest extent, depending on the product selected (Bastinet et al., 2017). Further, canopy height is a major determining factor in selecting harvest or conservation areas and these model errors could potentially lead to misinformed local forest management decisions (Chazdon et al., 2016). In the context of coastal flood protection, mangrove forest density/cover improves flood buffering capacity and consistent monitoring over time will provide consistent and precise estimates for superior disaster planning (Menéndez, Losada, Torres-Ortega, Narayan, Beck). The broad relationship between cover and forest height suggests a similar flood buffering capacity may be observed in taller mangrove forests.

4.2. National scale

Inconsistent forest height estimates did not translate to dramatically different estimates of area-wide AGB – an encouraging finding for adopting a diverse array of sensors, depending on data availability, for national carbon accounting (Fatyoinboet et al., 2017), (Duncanson et al., 2020). The most important factor to consider at the national scale is the availability of representative forest plot data to ensure the accuracy of remote sensing-based AGB predictions (Chen et al., 2015, Fassnacht et al., 2014, Hill et al., 2013, Ketterings et al., 2001, Vorster, Evangelista, Stovall, Ex).

Interestingly, even in the absence of field data or spatially explicit estimates (e.g. IPCC), average mangrove biomass density provided unbiased total AGB estimates (in this case). The accuracy of IPCC estimates is encouraging from a mangrove biomass and accounting perspective (~12% from locally calibrated remote sensing-based totals), particularly with the inclusion of mangroves within payment for ecosystem service (PES) schemes such as REDD+, since nominally attributed values are deemed to be generally representative of reality (Reducing Emissions from D, 2013), (Miles and Kapos, 1454). Middle and low income countries make up the majority of mangrove holding nations and forest area (Giriet al., 2011), (Bunting et al., 2018), but may be less likely to prioritize expensive field data for improved calibration models. In these cases, the use of the IPCC estimates for regional and national reporting is encouraging, but should be more thoroughly evaluated in other countries. Regardless of the accuracy, the high true uncertainty (based on validation) of IPCC totals (~130%) is still a major barrier limiting their application in the context of PES, which reduce valuations as AGB uncertainty increases (Global Forest Observation, 2016).

Spatially explicit estimates made with locally calibrated AGB models were essential to reducing uncertainty in area-wide total mangrove AGB, underscoring the importance of applying remote sensing-based mapping of AGB for carbon accounting, whenever feasible (White et al., 2016). In contrast, the global mangrove AGB model (Simard et al.) was ~40% biased in every height class in comparison to the locally calibrated estimates. After a direct comparison of AGB predictions from our local allometric model, we can clearly attribute this consistent bias to a global allometric height-biomass model calibrated without reference data representing the forest heights observed in Pongara National Park (maximum observed plot height in the Simard et al. study was ~40 m; Fig. 10). In the same respect, application of regional calibration models outside of the specific forest systems can result in bias, altering the total estimates AGB in a forest (Mitchard et al., 2014). In short, both regional and global AGB products must be locally re-calibrated and validated before being taken as “truth” at the local or national scale (Huanget al., (McRoberts et al., 2019).

4.3. Global scale

The next generation of global mangrove forest structure (height and AGB) products will need to address three major challenges: (Houghton, Hall, Goetz) reducing uncertainty in remotely sensed heights covering

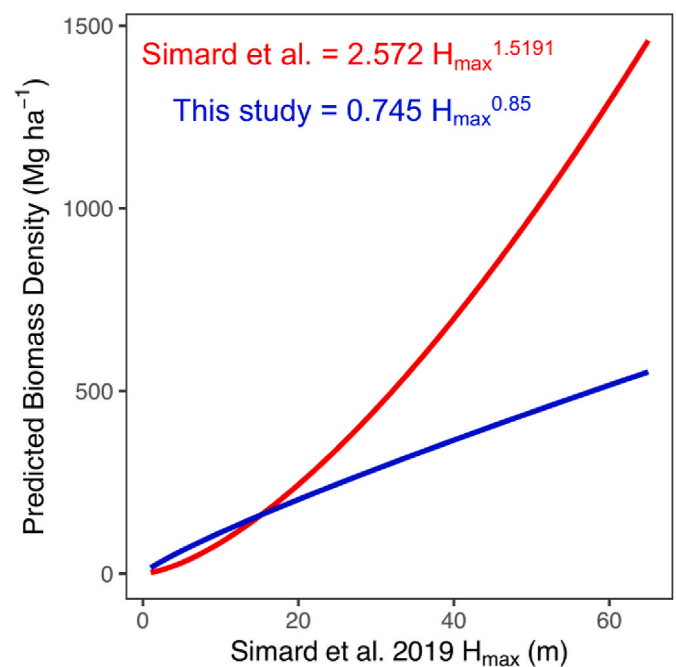


Fig. 10. Comparison between Simard et al. (Simard et al.) global H_{max} biomass predictions (red) and the locally calibrated H_{max} model developed in this study (blue). (For interpretation of the references to color in this figure legend, the reader is referred to the Web version of this article.)

the vast majority of mangrove area (Panet al., 2011), ensuring representativeness of sparse plot data and AGB allometry, and (Bonan, 2008) understanding of factors controlling secondary structure variables beyond height that directly influence AGB (e.g. basal area).

Approximately 95% of all mangrove forests are below 40 m in height with a global median of ~13 m – around 50% of global mangrove area has between 50 and 70% uncertainty in remotely sensed height estimates (Simard et al.). In effect, our findings of substantial disagreement in height estimates across sensors for the most common height range of mangroves globally suggests a universal field-based plot height-biomass allometry cannot be confidently applied across sensors. Yet, the comparisons made here provide clear expectations for the biases for each height product and the potential for cross calibration (Duncanson et al., 2020). The near-linear height biomass relationship present across most remote sensing products in this study suggests cross-calibration is possible with a maximum total uncertainty of ~50–100 Mg ha^{-1} . Similar to the disagreements in height, relative variations in AGB predictions across products was high in short stature forests (<15 m), reaching between 50 and 200%. Given the high cross sensor variability it is critical global continuous height products be created with rigorously validated and spatially continuous height products (e.g. TanDEM-X). Moreover, the key to global validation of canopy height is likely to come with spaceborne LiDAR sensors (e.g. GEDI; (Dubayah et al.)) with direct ground detection – a major limitation with PolInSAR height estimates in other forests with topography (Qi and Dubayah, 2016).

Global AGB calibration datasets are sparse and likely have unrepresentative tree-level allometric estimates of biomass (Mitchard et al., 2014), (Chave et al., 2014), (Stovall et al., 2018) (Fig. 10). The most exhaustive remotely sensed mangrove specific AGB map to date used 332 AGB field plots to calibrate ICESat-GLAS adjusted SRTM data (Simard et al.). Spatial biases are especially prevalent in the global calibration dataset, with 45% of plot data from a single country (Bangladesh). Simard et al. (Simard et al.) compared several regional allometric relationships with significant biases. They did not have allometry for the Atlantic coast of Africa which may be reflected in the observed biases. Improved plot-level calibration data is clearly needed

to improve the predictions of global models (Rovaiet al., 2021). Sensor calibration in unique forest ecosystems is limited by a lack of unrepresentative plot-based calibration data (i.e. plot-level biomass estimates may be inaccurate due to biased tree-level allometry; (Domke et al., 2012), (Duncanson, Huang, Johnson, Swatantran, McRoberts, Dubayah)). Here, we constrained our analysis to a single allometric equation (Chave et al., 2014), but the representativeness of this equation in such an understudied ecosystem remains unknown (Fatoyinbo et al., 2018), (Feliciano, Wdowinski, Potts, Lee, Fatoyinbo). Our evaluation of variation due to plot-level allometric biomass estimates using the Komiyama et al. (Komiyama, Pongpam, Kato) equation highlights the potential for a propagation of changes in plot-based calibration by a simple change in tree-level allometry (Vorster, Evangelista, Stovall, Ex). In protected and unique systems, as found in Pongara National Park, non-destructive allometric equations with novel technologies (e.g. Terrestrial Laser Scanning; (Calders et al.)) can bridge a critical gap in our understanding of scaling relationships without detrimentally impacting the study system (Stovall et al., 2018), (Feliciano et al., 2014), (Stovall et al., 2019). Future work should focus on updating these scaling relationships (Olagokeet al., 2016) and assessing their impact on sensor calibration (Stovall and Shugart, 2018) to better predict changes in forest biomass over time (Lagomasino et al., 2019), (Harris et al., 2021), (Richards, Thompson, Wijedasa).

Major advances in global AGB modeling in mangrove systems will come with the inclusion of measured or modeled secondary structural variables. Only approximately half of the variation in global AGB models can be explained by height alone (Simard et al.), suggesting secondary axes of variation (e.g. basal area, stem density, regional allometry) will substantially improve mapped AGB. Of the available plot data, efforts to understand the drivers in spatial variability of these secondary structural characteristics will be key in precisely capturing AGB at a global scale.

Moving forward – especially in the context of this “golden age” of forest-focused active remote sensing – the findings of this study enable sensor cross calibration for consistent monitoring of forest function. Calibrated forest height is a key physiological variable representing organismal function beyond biomass alone (e.g. moderate disturbance: (Atkinset al., 2020); hurricane damage (Lagomasino et al., 2020, Atkinset al., 2020, Taillie et al., 2017); drought susceptibility: (Stovall, Shugart, Yanga, Stovall, Shugart, Yangb, McGregoret al., 2020)). With the sensor evaluation performed here we gain the ability to monitor three-dimensional structural change across sensors in mangrove forest systems globally by matching past spaceborne missions (e.g. SRTM) with ongoing (e.g. TanDEM-X, GEDI and ICESat-2) and future (e.g. BIOMASS or NISAR) missions.

Declaration of competing interest

The authors declare that they have no known competing financial interests or personal relationships that could have appeared to influence the work reported in this paper.

Acknowledgements

This work was funded by the NASA Postdoctoral Program Fellowship and the NASA Carbon Monitoring System Program Project “Estimating Total Ecosystem Carbon in Blue Carbon and Tropical Peatland Ecosystems (16-CMS16-0073).

Appendix A. Supplementary data

Supplementary data to this article can be found online at <https://doi.org/10.1016/j.srs.2021.100034>.

References

- IPCC, 2006. IPCC Guidelines for National Greenhouse Gas Inventories. IGES, Japan, 2006, [Online]. Available: <http://www.ipcc-nggip.iges.or.jp/public/2006gl/index.html>.
- Abdalati, W., et al., May 2010. The ICESat-2 laser altimetry mission. Proc. IEEE 98 (5), 735–751. <https://doi.org/10.1109/JPROC.2009.2034765>.
- Armstrong, J., et al., 2020. AfriSAR: Gridded Forest Biomass and Canopy Metrics Derived from LVIS, Gabon, 2016. ORNL Distributed Active Archive Center. <https://doi.org/10.3334/ORNLDAAC/1775>.
- Aslan, A., Rahman, A.F., Robeson, S.M., 2018. Investigating the use of Alos Prism data in detecting mangrove succession through canopy height estimation. Ecol. Indic. 87, 136–143. <https://doi.org/10.1016/j.ecolind.2017.12.008>.
- Atkins, J.W., et al., 2020. Application of multidimensional structural characterization to detect and describe moderate forest disturbance. Ecosphere 11 (6), e03156. <https://doi.org/10.1002/ecs2.3156>.
- Avitabile, V., et al., Apr. 2016. An integrated pan-tropical biomass map using multiple reference datasets. Global Change Biol. 22 (4), 1406–1420. <https://doi.org/10.1111/gcb.13139>.
- Barbier, E.B., Aug. 2016. The protective service of mangrove ecosystems: a review of valuation methods. Mar. Pollut. Bull. 109 (2), 676–681. <https://doi.org/10.1016/j.marpolbul.2016.01.033>.
- Bastin, J.-F., et al., May 2017. The extent of forest in dryland biomes. Science 356 (6338), 635–638. <https://doi.org/10.1126/science.aam6527>.
- Blair, J.B., Rabine, D.L., Hofton, M.A., Jul. 1999. The Laser Vegetation Imaging Sensor: a medium-altitude, digitisation-only, airborne laser altimeter for mapping vegetation and topography. Isprs J. Photogramm. Remote Sens. 54 (2–3), 115–122. [https://doi.org/10.1016/S0924-2716\(99\)00002-7](https://doi.org/10.1016/S0924-2716(99)00002-7).
- Bonan, G.B., 2008. Forests and climate change: forcings, feedbacks, and the climate benefits of forests. Science 320 (5882), 1444–1449.
- Bunting, P., et al., Oct. 2018. The global mangrove watch—a new 2010 global baseline of mangrove extent. Rem. Sens. 10 (10), 1669. <https://doi.org/10.3390/rs10101669>.
- Calders, K., et al., Dec. 2020. Terrestrial laser scanning in forest ecology: expanding the horizon. Remote Sens. Environ. 251, 112102. <https://doi.org/10.1016/j.rse.2020.112102>.
- Chave, J., et al., 2014. Improved allometric models to estimate the aboveground biomass of tropical trees. Global Change Biol. 20 (10), 3177–3190.
- Chazdon, R.L., et al., Sep. 2016. When is a forest a forest? Forest concepts and definitions in the era of forest and landscape restoration. Ambio 45 (5), 538–550. <https://doi.org/10.1007/s13280-016-0772-y>.
- Chen, Q., Vaglio Laurin, G., Valentini, R., Apr. 2015. Uncertainty of remotely sensed aboveground biomass over an African tropical forest: propagating errors from trees to plots to pixels. Remote Sens. Environ. 160, 134–143. <https://doi.org/10.1016/j.rse.2015.01.009>.
- Cohen, R., et al., Dec. 2013. Propagating uncertainty to estimates of above-ground biomass for Kenyan mangroves: a scaling procedure from tree to landscape level. For. Ecol. Manag. 310, 968–982. <https://doi.org/10.1016/j.foreco.2013.09.047>.
- Dauby, G., Leal, M., Stévant, T., 2008. Vascular plant checklist of the coastal national Park of Pongara. Gabon, 63.
- Denbina, M., Simard, M., Hawkins, B., Oct. 2018. Forest height estimation using multibaseline PolInSAR and sparse lidar data fusion. IEEE J. Sel. Top. Appl. Earth Obs. Remote Sens. 11 (10), 3415–3433. <https://doi.org/10.1109/JSTARS.2018.2841388>.
- Domke, G.M., Woodall, C.W., Smith, J.E., Westfall, J.A., McRoberts, R.E., Apr. 2012. Consequences of alternative tree-level biomass estimation procedures on U.S. forest carbon stock estimates. For. Ecol. Manag. 270, 108–116. <https://doi.org/10.1016/j.foreco.2012.01.022>.
- Donato, D.C., Kauffman, J.B., Murdiyarsa, D., Kurnianto, S., Stidham, M., Kanninen, M., May 2011. Mangroves among the most carbon-rich forests in the tropics. Nat. Geosci. 4 (5), 293–297. <https://doi.org/10.1038/NNGEO1123>.
- Dubayah, R., et al., Jun. 2020. The global ecosystem Dynamics investigation: high-resolution laser ranging of the Earth’s forests and topography. Sci. Remote Sens. 1, 100002. <https://doi.org/10.1016/j.srs.2020.100002>.
- Duncanson, L., Huang, W., Johnson, K., Swatantran, A., McRoberts, R.E., Dubayah, R., Oct. 2017. Implications of allometric model selection for county-level biomass mapping. Carbon Bal. Manag. 12 (1), 18. <https://doi.org/10.1186/s13021-017-0086-9>.
- Duncanson, L., et al., 2020. Biomass estimation from simulated GEDI, ICESat-2 and NISAR across environmental gradients in Sonoma County, California. Remote Sens. Environ. 242, 111779. <https://doi.org/10.1016/j.rse.2020.111779>.
- Ewel, K., Twilley, R., Ong, J., 1998. Different kinds of mangrove forests provide different goods and services. Global Ecol. Biogeogr. Lett. 7 (1), 83–94.
- Farr, T.G., et al., 2007. The Shuttle radar topography mission. Rev. Geophys. 45, 2. <https://doi.org/10.1029/2005RG000183>.
- Fassnacht, F.E., et al., 2014. Importance of sample size, data type and prediction method for remote sensing-based estimations of aboveground forest biomass. Remote Sens. Environ. 154, 102–114. <https://doi.org/10.1016/j.rse.2014.07.028>.
- Fatoyinbo, T.E., Simard, M., 2013. Height and biomass of mangroves in Africa from ICESat/GLAS and SRTM. Int. J. Rem. Sens. 34 (2), 668–681. <https://doi.org/10.1080/01431161.2012.712224>.
- Fatoyinbo, T., Feliciano, E.A., Lagomasino, D., Lee, S.K., Trettin, C., Feb. 2018. Estimating mangrove aboveground biomass from airborne LiDAR data: a case study from the Zambezi River delta. Environ. Res. Lett. 13 (2), 25012. <https://doi.org/10.1088/1748-9326/aa9f03>.
- Fatoyinbo, L., et al., 2017. The 2016 NASA AfriSAR campaign: airborne SAR and Lidar measurements of tropical forest structure and biomass in support of future satellite

- missions. 2017 IEEE International Geoscience and Remote Sensing Symposium. IGARSS), pp. 4286–4287.
- Fatoyinbo, T., et al., 2021. The NASA AfriSAR campaign: airborne SAR and lidar measurements of tropical forest structure and biomass in support of current and future space missions. *Remote Sens. Environ.* 264, 112533. <https://doi.org/10.1016/j.rse.2021.112533>.
- Feliciano, E.A., Wdowski, S., Potts, M.D., Oct. 2014. Assessing mangrove above-ground biomass and structure using terrestrial laser scanning: a case study in the everglades national Park. *Wetlands* 34 (5), 955–968. <https://doi.org/10.1007/s13157-014-0558-6>.
- Feliciano, E.A., Wdowski, S., Potts, M.D., Lee, S.-K., Fatoyinbo, T.E., Jul. 2017. Estimating mangrove canopy height and above-ground biomass in the everglades national Park with airborne LiDAR and TanDEM-X data. *Rem. Sens.* 9 (7), 702. <https://doi.org/10.3390/rs9070702>.
- Giri, C., et al., 2011. Status and distribution of mangrove forests of the world using earth observation satellite data: status and distributions of global mangroves. *Global Ecol. Biogeogr.* 20 (1), 154–159. <https://doi.org/10.1111/j.1466-8238.2010.00584.x>.
- Global Forest Observations Initiative, 2016. Integration of Remote-Sensing and Ground-Based Observations for Estimation of Emissions and Removals of Greenhouse Gases in Forests: Methods and Guidance from the Global Forest Observations Initiative, Edition 2.0, vol. 224. "UN Food Agric. Organ.", pp 1–224
- Goldberg, L., Lagomasino, D., Thomas, N., Fatoyinbo, T., 2020. Global declines in human-driven mangrove loss. *Global Change Biol.* n/a <https://doi.org/10.1111/gcb.15275> n/a.
- Gopal, B., Chauhan, M., 2006. Biodiversity and its conservation in the Sundarban mangrove ecosystem. *Aquat. Sci.* 68 (3), 338–354.
- Harding, D.J., Lefsky, M.A., Parker, G.G., Blair, J.B., Jun. 2001. Laser altimeter canopy height profiles - methods and validation for closed-canopy, broadleaf forests. *Remote Sens. Environ.* 76 (3), 283–297. [https://doi.org/10.1016/S0034-4257\(00\)00210-8](https://doi.org/10.1016/S0034-4257(00)00210-8).
- Harris, N.L., et al., 2021. Global maps of twenty-first century forest carbon fluxes. *Nat. Clim. Change*, Jan. <https://doi.org/10.1038/s41558-020-00976-6>.
- Hensley, S., et al., May 2008. The UAVSAR Instrument: Description and First Results. In: 2008 IEEE Radar Conference, Rome, Italy, pp. 1–6. <https://doi.org/10.1109/RADAR.2008.4720722>.
- Hill, T.C., Williams, M., Bloom, A.A., Mitchard, E.T.A., Ryan, C.M., Sep. 2013. Are inventory based and remotely sensed above-ground biomass estimates consistent? *PLoS One* 8 (9), e74170. <https://doi.org/10.1371/journal.pone.0074170>.
- Horn, R., Nottensteiner, A., Reigber, A., Fischer, J., Scheiber, R., 2009. F-SAR - DLR's new multifrequency polarimetric airborne SAR. In: 2009 IEEE International Geoscience and Remote Sensing Symposium, Cape Town, South Africa. <https://doi.org/10.1109/IGARSS.2009.5418244> p. II-902-II-905.
- Houghton, R.A., Hall, F., Goetz, S.J., Sep. 2009. Importance of biomass in the global carbon cycle. *J. Geophys. Res.-Biogeosciences* 114, G00E03. <https://doi.org/10.1029/2009JG000935>.
- Huang, W., et al., Dec. 2015. Local discrepancies in continental scale biomass maps: a case study over forested and non-forested landscapes in Maryland, USA. *Carbon Bal. Manag.* 10, 19. <https://doi.org/10.1186/s13021-015-0030-9>.
- Jetz, W., et al., Apr. 2019. Essential biodiversity variables for mapping and monitoring species populations. *Nat. Ecol. Evol.* 3 (4), 539–551. <https://doi.org/10.1038/s41559-019-0826-1>.
- Kauffman, J.B., et al., May 2020. Total ecosystem carbon stocks of mangroves across broad global environmental and physical gradients. *Ecol. Monogr.* 90 (2) <https://doi.org/10.1002/ecm.1405>.
- Ketterings, Q.M., Coe, R., van Noordwijk, M., Ambagau, Y., Palm, C.A., Jun. 2001. Reducing uncertainty in the use of allometric biomass equations for predicting above-ground tree biomass in mixed secondary forests. *For. Ecol. Manag.* 146 (1–3), 199–209. [https://doi.org/10.1016/S0378-1127\(00\)00460-6](https://doi.org/10.1016/S0378-1127(00)00460-6).
- Komiyama, A., Pongpan, S., Kato, S., Jul. 2005. Common allometric equations for estimating the tree weight of mangroves. *J. Trop. Ecol.* 21 (4), 471–477. <https://doi.org/10.1017/S0266467405002476>.
- Krieger, G., et al., 2007. TanDEM-X: a satellite formation for high-resolution SAR interferometry. *IEEE Trans. Geosci. Rem. Sens.* 45 (11), 3317–3341. <https://doi.org/10.1109/TGRS.2007.900693>. Nov.
- Krieger, G., et al., Aug. 2013. TanDEM-X: a radar interferometer with two formation-flying satellites. *Acta Astronaut.* 89, 83–98. <https://doi.org/10.1016/j.actaastro.2013.03.008>.
- Lagomasino, D., Fatoyinbo, T., Lee, S., Feliciano, E., Trettin, C., Simard, M., Apr. 2016. A comparison of mangrove canopy height using multiple independent measurements from land, air, and space. *Rem. Sens.* 8 (4), 327. <https://doi.org/10.3390/rs8040327>.
- Lagomasino, D., et al., Jan. 2019. Measuring mangrove carbon loss and gain in deltas. *Environ. Res. Lett.* 14 (2), 25002. <https://doi.org/10.1088/1748-9326/aaaf0de>.
- Lagomasino, D., et al., 2020. Storm surge, not wind, caused mangrove dieback in southwest Florida following Hurricane Irma. <https://doi.org/10.31223/osf.io/q4exh>. Jul.
- R Core Team, 2019. R: A Language and Environment for Statistical Computing. R Foundation for Statistical Computing, Vienna, Austria [Online]. Available: <https://www.R-project.org/>.
- Le Quéré, C., et al., 2017. Global carbon budget 2017. *Earth Syst. Sci. Data Discuss.* 1–79. <https://doi.org/10.5194/essd-2017-123>. Nov.
- Le Toan, T., et al., 2011. The BIOMASS mission: mapping global forest biomass to better understand the terrestrial carbon cycle. *Remote Sens. Environ.* 115 (11), 2850–2860. <https://doi.org/10.1016/j.rse.2011.03.020>. Nov.
- Lee, S.-K., Fatoyinbo, T.E., Lagomasino, D., Feliciano, E., Trettin, C., Oct. 2018. Multibaseline TanDEM-X mangrove height estimation: the selection of the vertical wavenumber. *IEEE J. Sel. Top. Appl. Earth Obs. Remote Sens.* 11 (10), 3434–3442. <https://doi.org/10.1109/JSTARS.2018.2835647>.
- Lucas, R., et al., Feb. 2020. Structural characterisation of mangrove forests achieved through combining multiple sources of remote sensing data. *Remote Sens. Environ.* 237, 111543. <https://doi.org/10.1016/j.rse.2019.111543>.
- Lucas, R., et al., 2017. Spatial ecology of mangrove forests: a remote sensing perspective. In: Rivera-Monroy, V.H., Lee, S.Y., Kristensen, E., Twilley, R.R. (Eds.), "in *Mangrove Ecosystems: A Global Biogeographic Perspective: Structure, Function, and Services*. Springer International Publishing, Cham, pp. 87–112. https://doi.org/10.1007/978-3-319-62206-4_4.
- McGregor, I.R., et al., 2020. Tree height and leaf drought tolerance traits shape growth responses across droughts in a temperate broadleaf forest. *New Phytol.* <https://doi.org/10.1111/nph.16996>.
- McLeod, E., et al., Dec. 2011. A blueprint for blue carbon: toward an improved understanding of the role of vegetated coastal habitats in sequestering CO₂. *Front. Ecol. Environ.* 9 (10), 552–560. <https://doi.org/10.1890/110004>.
- McRoberts, R.E., Næsset, E., Saatchi, S., Liknes, G.C., Walters, B.F., Chen, Q., 2019. Local validation of global biomass maps. *Int. J. Appl. Earth Obs. Geoinformation* 83, 101931. <https://doi.org/10.1016/j.jag.2019.101931>. Nov.
- Menéndez, P., Losada, I.J., Torres-Ortega, S., Narayan, S., Beck, M.W., Dec. 2020. The global flood protection benefits of mangroves. *Sci. Rep.* 10 (1) <https://doi.org/10.1038/s41598-020-61136-6>.
- Miles, L., Kapos, V., 2008. Reducing greenhouse gas emissions from deforestation and forest degradation: global land-use implications. *Science* 320 (5882), 1454–1455. <https://doi.org/10.1126/science.1155358>. Jun.
- Mitchard, E.T.A., et al., 2012. Mapping tropical forest biomass with radar and spaceborne LiDAR in Lope National Park, Gabon: overcoming problems of high biomass and persistent cloud. *Biogeosciences* 9 (1), 179–191. <https://doi.org/10.5194/bg-9-179-2012>.
- Mitchard, E.T.A., et al., Aug. 2014. Markedly divergent estimates of Amazon forest carbon density from ground plots and satellites. *Global Ecol. Biogeogr.* 23 (8), 935–946. <https://doi.org/10.1111/geb.12168>.
- Olagoe, A., et al., 2016. Extended biomass allometric equations for large mangrove trees from terrestrial LiDAR data. *Trees (Berl.)* 30 (3), 935–947. <https://doi.org/10.1007/s00468-015-1334-9>.
- Ouyang, X., Lee, S.Y., Dec. 2020. Improved estimates on global carbon stock and carbon pools in tidal wetlands. *Nat. Commun.* 11 (1) <https://doi.org/10.1038/s41467-019-14120-2>.
- Pan, Y., et al., Aug. 2011. A large and persistent carbon sink in the world's forests. *Science* 333 (6045), 988–993. <https://doi.org/10.1126/science.1201609>.
- Pardini, M., Tello, M., Cazcarra-Bes, V., Papathanassiou, K.P., Hajnsek, I., Oct. 2018. L- and P-band 3-D SAR reflectivity profiles versus lidar waveforms: the AfriSAR case. *IEEE J. Sel. Top. Appl. Earth Obs. Remote Sens.* 11 (10), 3386–3401. <https://doi.org/10.1109/JSTARS.2018.2847033>.
- Qi, W., Dubayah, R.O., Dec. 2016. Combining Tandem-X InSAR and simulated GEDI lidar observations for forest structure mapping. *Remote Sens. Environ.* 187, 253–266. <https://doi.org/10.1016/j.rse.2016.10.018>.
- Reducing emissions from deforestation and forest degradation (Program), food and agriculture Organization of the united nations, united nations Development programme, and united nations environment programme. In: National Forest Monitoring Systems: Monitoring and Measurement, Reporting and Verification (M & MRV) in the Context of REDD+ Activities, 2013. UN-REDD Programme Secretariat, Geneva.
- Richards, D.R., Thompson, B.S., Wijedasa, L., Dec. 2020. Quantifying net loss of global mangrove carbon stocks from 20 years of land cover change. *Nat. Commun.* 11 (1) <https://doi.org/10.1038/s41467-020-18118-z>.
- Rosen, P., et al., Jul. 2016. An update on the NASA-ISRO dual-frequency DBF SAR (NISAR) mission. In: 2016 IEEE International Geoscience and Remote Sensing Symposium. IGARSS), Beijing, China, pp. 2106–2108. <https://doi.org/10.1109/IGARSS.2016.7729543>.
- Rovai, A.S., et al., 2021. Macroecological patterns of forest structure and allometric scaling in mangrove forests. *Glob. Ecol. Biogeogr.* <https://doi.org/10.1111/geb.13268>.
- Roy, D.P., Kashongwe, H.B., Armston, J., Dec. 2021. The impact of geolocation uncertainty on GEDI tropical forest canopy height estimation and change monitoring. *Sci. Remote Sens.* 4, 100024. <https://doi.org/10.1016/j.srs.2021.100024>.
- Saatchi, S.S., et al., 2019. AfriSAR: Aboveground Biomass for Lope, Mabounie, Mondah, and Rabi Sites, Gabon. ORNL Distributed Active Archive Center. <https://doi.org/10.3334/ORNLDAA/1681>.
- Sanderan, J., et al., May 2018. A global map of mangrove forest soil carbon at 30 m spatial resolution. *Environ. Res. Lett.* 13 (5), 55002. <https://doi.org/10.1088/1748-9326/aabe1c>.
- Santoro, M., et al., Oct. 2015. Forest growing stock volume of the northern hemisphere: spatially explicit estimates for 2010 derived from Envisat ASAR. *Remote Sens. Environ.* 168, 316–334. <https://doi.org/10.1016/j.rse.2015.07.005>.
- Sexton, J.O., Bax, T., Siqueira, P., Swenson, J.J., Hensley, S., 2009. A comparison of lidar, radar, and field measurements of canopy height in pine and hardwood forests of southeastern North America. *For. Ecol. Manag.* 257 (3), 1136–1147. <https://doi.org/10.1016/j.foreco.2008.11.022>.
- Simard, M., Rivera-Monroy, V.H., Mancera-Pineda, J.E., Castañeda-Moya, E., Twilley, R.R., May 2008. A systematic method for 3D mapping of mangrove forests based on Shuttle Radar Topography Mission elevation data, ICESat/GLAS waveforms and field data: application to Ciénaga Grande de Santa Marta, Colombia. *Remote Sens. Environ.* 112 (5), 2131–2144. <https://doi.org/10.1016/j.rse.2007.10.012>.

- Simard, M., et al., Jan. 2019. Mangrove canopy height globally related to precipitation, temperature and cyclone frequency. *Nat. Geosci.* 12 (1), 40–45. <https://doi.org/10.1038/s41561-018-0279-1>.
- Stovall, A.E.L., Shugart, H.H., Oct. 2018. Improved biomass calibration and validation with terrestrial LiDAR: implications for future LiDAR and SAR missions. *IEEE J. Sel. Top. Appl. Earth Obs. Remote Sens.* 11 (10), 3527–3537. <https://doi.org/10.1109/JSTARS.2018.2803110>.
- Stovall, A.E.L., Anderson-Teixeira, K.J., Shugart, H.H., 2018. Assessing terrestrial laser scanning for developing non-destructive biomass allometry. *For. Ecol. Manag.* 427, 217–229. <https://doi.org/10.1016/j.foreco.2018.06.004>. Nov.
- Stovall, A.E.L., Diamond, J.S., Slesak, R.A., McLaughlin, D.L., Shugart, H., 2019. Quantifying wetland microtopography with terrestrial laser scanning. *Remote Sens. Environ.* 232, 111271. <https://doi.org/10.1016/j.rse.2019.111271>.
- Stovall, A.E.L., Shugart, H., Yang, X., Sep. 2019. Tree height explains mortality risk during an intense drought. *Nat. Commun.* 10 (1), 4385. <https://doi.org/10.1038/s41467-019-12380-6>.
- Stovall, A.E.L., Shugart, H.H., Yang, X., Jul. 2020. Reply to 'Height-related changes in forest composition explain increasing tree mortality with height during an extreme drought'. *Nat. Commun.* 11 (1), 3401. <https://doi.org/10.1038/s41467-020-17214-4>.
- Tadono, T., Ishida, H., Oda, F., Naito, S., Minakawa, K., Iwamoto, H., Apr. 2014. Precise global DEM generation by ALOS PRISM. *ISPRS Ann. Photogramm. Remote Sens. Spat. Inf. Sci.* II (4), 71–76. <https://doi.org/10.5194/isprsannals-II-4-71-2014>.
- P. J. Taillie et al., "Widespread mangrove damage resulting from the 2017 Atlantic mega hurricane season," *Environ. Res. Lett.*, vol. 15, no. 6, p. 64010, Jun. 2020, doi: 10.1088/1748-9326/ab82cf.
- Thomas, N., Lucas, R., Bunting, P., Hardy, A., Rosenqvist, A., Simard, M., 2017. Distribution and drivers of global mangrove forest change, 1996–2010. *PLoS One* 12 (6).
- Trettin, C.C., et al., 2020. Carbon Stock Inventory of Mangroves, Pongara National Park. Forest Service Research Data Archive., Gabon. Fort Collins, CO <https://doi.org/10.2737/rds-2020-0040>.
- Trettin, C.C., et al., May 2021. Mangrove carbon stocks in Pongara national Park, Gabon. *Estuar. Coast Shelf Sci.* 107432. <https://doi.org/10.1016/j.ecss.2021.107432>.
- Ucar, I., Pebesma, E., Azcorra, A., 2019. Measurement errors in R. *R. J.* 10 (2), 549. <https://doi.org/10.32614/RJ-2018-075>.
- Vorster, A.G., Evangelista, P.H., Stovall, A.E.L., Ex, S., Dec. 2020. Variability and uncertainty in forest biomass estimates from the tree to landscape scale: the role of allometric equations. *Carbon Bal. Manag.* 15 (1) <https://doi.org/10.1186/s13021-020-00143-6>.
- White, J.C., Coops, N.C., Wulder, M.A., Vastaranta, M., Hilker, T., Tompalski, P., 2016. Remote sensing technologies for enhancing forest inventories: a review. *Can. J. Rem. Sens.* 42 (5), 619–641. <https://doi.org/10.1080/07038992.2016.1207484>. Sep.
- Worthington, T., Spalding, M., 2018. *Mangrove restoration potential*, p. 36.
- Worthington, T.A., et al., Dec. 2020. A global biophysical typology of mangroves and its relevance for ecosystem structure and deforestation. *Sci. Rep.* 10 (1) <https://doi.org/10.1038/s41598-020-71194-5>.
- Zeng, Y., Friess, D.A., Sarira, T.V., Siman, K., Koh, L.P., 2021. Global potential and limits of mangrove blue carbon for climate change mitigation. *Curr. Biol.* <https://doi.org/10.1016/j.cub.2021.01.070>.
- Zwally, H.J., et al., Oct. 2002. ICESat's laser measurements of polar ice, atmosphere, ocean, and land. *J. Geodyn.* 34 (3–4), 405–445. [https://doi.org/10.1016/S0264-3707\(02\)00042-X](https://doi.org/10.1016/S0264-3707(02)00042-X).